Escola de Camins
Escola Tècnica Superior d'Enginyeria de Camins, Canals i Ports
UPC BARCELONATECH

TESI DE MÀSTER

Màster

Màster en Enginyeria Estructural i de la Construcció

Títol

Shear Resistance of different Web Panels Of Linearly Tapered Bridge Girders With Steel Corrugated Webs

Autor

Eddy Jesus Zevallos Barrios

Tutor

Enrique Mirambell/Esther Real

Intensificació

Steel Structures

Data

3 febrer 2015

ACKNOWLEDGMENT

First and foremost I wish to thank my advisors, Professor Enrique Mirambell and Esther Real, Professors of Steel Structures of the engineering construction Area at UPC and professor Mostafa Hassanein of Tanta University from Egypt. They has been supportive since the days I began working on the origins as a master student; I remember she used to say something like "It does not matter if at the beginning you know nothing of the subject, perseveres and continues, in the end you will be who most know it.

Ever since, Ester, Enrique and Mostafa have supported me not only by providing a research assistantship over almost seven months, but also academically and emotionally through the rough road to finish this thesis. Thanks to them I had the opportunity to build truly friendship beyond the relation professor and student, and during the most difficult times when writing this thesis, they gave me the moral support and the freedom I needed to move on.

Agradecer a mi gran familia, que me han dado el soporte necesario desde que inicie en esta carrera de arduo trabajo. A mi madre y a mi padre, que con su ejemplo de perseverancia me han inculcado como afrontar la vida desde otra óptica, la estudiantil, lejos de la zona de confort familiar. A mis hermanos que han sabido cubrir el vacío familiar, que significa la distancia entre nosotros.

A mi novia, Katherine, en ella encontré la fuerza necesaria para continuar, para salir adelante ante la adversidad, gracias por todo el amor y paciencia que me diste. Agradezco a la familia Toledo Muñoz, que al igual que mi familia carnal, representan pieza fundamental en este logro, concretado con mucho esfuerzo.

A la familia Zevallos Hernani, su apoyo incondicional en Barcelona, han sido preponderante para el desarrollo de mis estudios, tía Patty, Karina y Jenny, gracias por los gratos momentos familiares, que me ayudaron a disipar en esos momentos de tensión, durante este periodo. Gracias por aceptarme en su núcleo familiar, como miembro de los suyos.

ABSTRACT

Although steel girders have been used for many years, new generation of optimized steel girders is developed by the advances in structural and fabrication technology. Girders with corrugated webs are used in bridges as an efficient alternative to conventional girders with flat stiffened webs, It was also found that, the vertically corrugated girders had a 10.6% reduction in weight when compared with the beam with flat web.[1]

Advantages Economical design of steel girders normally requires thin webs. The use of corrugated webs is a possible way of achieving adequate out-of-plane stiffness without using stiffeners. Particularly in bridge girders with corrugated webs (BGCWs), the corrugated webs are the main elements for bearing the shear forces. Instead of prismatic BGCWs, tapered BGCWs are currently used mainly due to their structural efficiency, providing at the same time aesthetical appearance.

Available literature shows that tapered BGCWs may be classified into four typologies. Among these typologies, Case I and Case II are the most common cases appearing commonly near to the intermediate supports of continuous bridges.

Accordingly, in this thesis, the finite element (FE) method is employed to investigate the inelastic behaviour of tapered BGCWs of Case I and Case II, following to the fundamental behaviour of such girders published recently by Hassanein et al [6].

The thesis seeks, firstly, considering initial imperfection amplitudes of $h_{w1}/200$. Accordingly, with euro code 3 part 1-5, annex D [12], h_{w1} is the height of the long vertical edge of the web panel, it investigates the effect of the aspect ratio of the web panels, different flange inclination angles and different web thickness.

Finally, the thesis checks previously proposed design model using the results of the generated parametric studies. Overall, the outcomes of this study are expected to provide more insight into the behaviour of tapered BGCWs and enable accurate prediction of the shear capacity of this special type of BGCWs.

INDEX

FIGURE INDEX

TABLES INDEX

SHEAR RESISTANCE OF DIFFERENT WEB PANELS OF LINEARLY TAPERED BRIDGE GIRDERS WITH STEEL CORRUGATED WEBS

Chapter 1. Introduction

1.1. General

In case of plate girders with slender webs, the web panel buckles at a relatively low value of the applied load. Hence, to overcome the strength reduction associated with utilizing plate girders with slender webs in bridge construction, these flat webs are often reinforced with transversal stiffeners along their spans to increase their buckling strength. Recently, girders with steel corrugated webs have been used as structural members in Bridges; for example see Figure. 1(a) which is presenting the Maupré Bridge in France [1].

Because of their significant out-of-plane stiffness, corrugated web plates have much higher buckling strengths compared with flat web plates. Hence, the necessity of using stiffeners is eliminated and the required web thickness is reduced [2-6]. Additionally, the flexural strength of such girders is entirely provided by their flanges while the shear strength is provided by their webs. This is attributed to the negligible axial stiffness of the corrugated webs in the longitudinal directions of the girders which is known as the accordion effect [7-8].

Consequently, there is no interaction between shear and flexural behaviors. For that reason, it is widely accepted to assume a constant shear stress in the corrugated webs of such girders and then to quantify it in terms of the average shear stress ($\tau = V / t_w h_w$); V is the vertical shear force of the girder, h_w represents the web depth and t_w stands for the web thickness.

On the other hand, tapered girders are currently used in bridges mainly due to their structural efficiency, providing at the same time aesthetical appearance. The Hondani Bridge in Japan is an example of the application of tapered bridge girder with steel corrugated webs (BGCWs) (Figure. 1(b)).

(a) Prismatic bridge girders

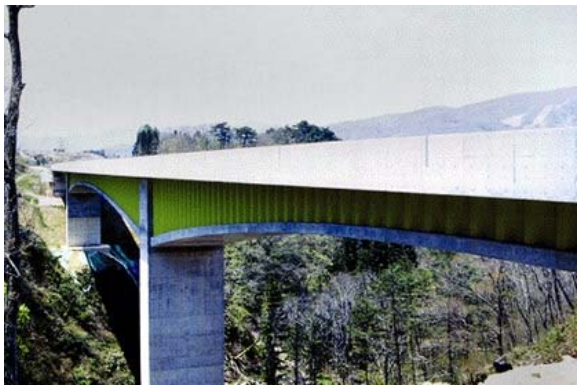

(b) Tapered bridge girders

Figure 1 Bridge girders with corrugated webs; (a) Maupré Bridge and (b) Hondani Bridge

Previous studies on tapered plate girders, by Bedynek et al. [9] and Hassanein and Kharoob [10], subjected to shear loading showed the existence of an additional vertical component derived from the axial force in the inclined flange. This phenomenon is called the "Resal effect". This makes their behaviour different from that of the prismatic girders. Owing to the lack of research thesis related to tapered BGCWs, this thesis provides the behaviour of different web panels existing in linearly tapered BGCWs.

1.2 Types of web panels in linearly tapered BGCWs

Figure. 2 shows the linearly tapered BGCWs considered in this investigation. As can be seen, it is a continuous bridge which composes from two spans. Based on previous researches [9,10], the web of this girder may be classified into three typologies.

This classification is based on (1) the inclination of the flange and whether the flange is under tension or compression and (2) the direction of the developed tension field, which may appear on the short or on the long web diagonal [9].

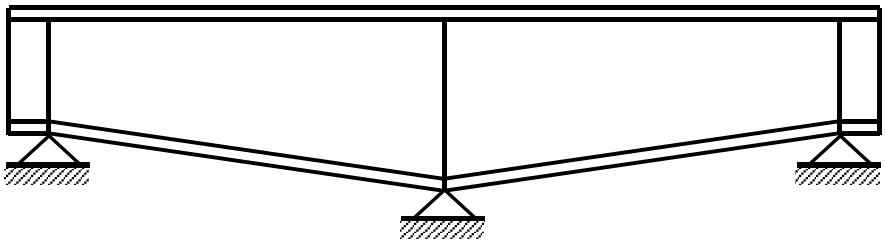

Figure 2 Linearly tapered BGCW

The check of shear of the girder shown in Figure. 2 should be preceded by an elastic analysis for the bending and shear of the girder. The purpose of such analysis is to determine the bending moment and shear force distributions throughout the girder, so that (1) the girder can be divided into different typologies and (2) the maximum shear forces can be found and compared with the shear capacities of each typology.

Figure. 3 provides the bending moment and shear force diagrams. According to the classification of the tapered girders into four typologies (based on the direction of the developed tension field and the type of the force in the inclined flange), this girder is composed of three typologies; I, II and IV. As can be seen from Figure. 3, the points of zero moment and zero shear divide the web into such typologies. It is worth pointing out that a forth typology (Case III) exists in another bridge layouts [10], as can be seen later.

1.2. Background of the problem

Because tapered BGCWs are used extensively as the main systems in modern bridges (Figure. 1(b)) without the availability of any source describing their shear buckling behavior, the current thesis studied the fundamental behaviour of such girders [10].

Research presented by Hassanein and Kharoob [10] focused, firstly, on the critical shear buckling stress (τ_{cr}) of the corrugated webs of tapered BGCWs. This was made by carrying

out elastic bifurcation buckling analyses using ABAQUS software [11] on isolated corrugated webs with simple and fixed boundary conditions.

Previous numerical studies presented in (Real et al., 2010; Bedynek et al., 2011) demonstrated that both critical load and ultimate strength of tapered plate girder are strongly influenced by two factors: (1) inclination of the flange and whether the flange is under tension or compression and (2) the direction of the developed tension field, which may appear on the short or on the long web diagonal.

As a result it is possible to distinguish four different typologies of tapered plate girders:

I. Inclined flange in compression and diagonal tension field developed in the short diagonal;
II. Inclined flange in tension and diagonal tension field developed in the long diagonal;
III. Inclined flange in tension and diagonal tension field developed in the short diagonal;
IV. Inclined flange in compression and diagonal tension field developed in the long diagonal.

Webs in different typologies of tapered girders with steel corrugated webs were considered; see Figure. 3. To reflect the behaviour of bridges, the corrugation dimensions of the considered corrugated webs were taken typical to those used previously in Shinkai and Matsnoki bridges. However, it was found that predicting τ_{cr} values for the tapered webs based on prismatic web (having the depth of the long vertical edge of the tapered web (h_{w1})) calculations is not accurate.

Therefore, critical buckling stresses ($\tau_{cr,\mathrm{Pr}op}$) for the tapered webs were proposed based on the stresses of prismatic webs, with different equation for each typology. The thesis [10] was, then, extended to investigate the nonlinear shear strengths of the tapered BGCWs. This was made based on the verifications made by the same authors on Ref. [6].

The aspect ratios of the web panels (a/h_{w1}) of the girders were 2.88, while the inclination angles were fixed to 7.125˚; a, h_{w1} are the shear span, the long vertical edge length. The flange slenderness was, additionally, constant throughout the investigation, while five web slenderness values were taken into consideration.

The available design shear strength formulas for prismatic girders (by Moon et al. [3] and Sause and Braxtan [12]) were compared with the FE shear strengths of the tapered BGCWs. Based on these comparisons, design strength ($\tau_{ul,\mathrm{Pr}op}$), based on the equation of Moon et al [3], for different tapered BGCWs cases was proposed, as follows:

$$\frac{\tau_{ul,\mathrm{Pr}op}}{\tau_y} = C_T \begin{cases} 1.0 & : \lambda_s \le 0.6 \\ 1-0.614(\lambda_s - 0.6) & : 0.6 < \lambda_s \le \sqrt{2} \\ \dfrac{1}{\lambda_s^2} & : \sqrt{2} < \lambda_s \end{cases} \quad (1)$$

where τ_y stands for the shear yielding strength of the steel material, λ_s represents the shear buckling parameter of the corrugated webs and C_T is taken as unity for cases I and II or as the ratio h_{wo}/h_{wi} for cases III and IV; h_{wo}/h_{wi} is ratio between the short vertical edge of the web panel to the long edge.

It is worth pointing out that the parameter λ_s uses, in its calculation, the $\tau_{cr,\mathrm{Prop}}$ value of each typology; for more details refer to reference [10]. According to the dimensions of Shinkai bridge with different web thickness used in [10], almost of the models had a parameter λ_s less than 0.6 (16 out of 20 models). The rest of models had a parameter λ_s just bigger than 0.6 (only 4 models).

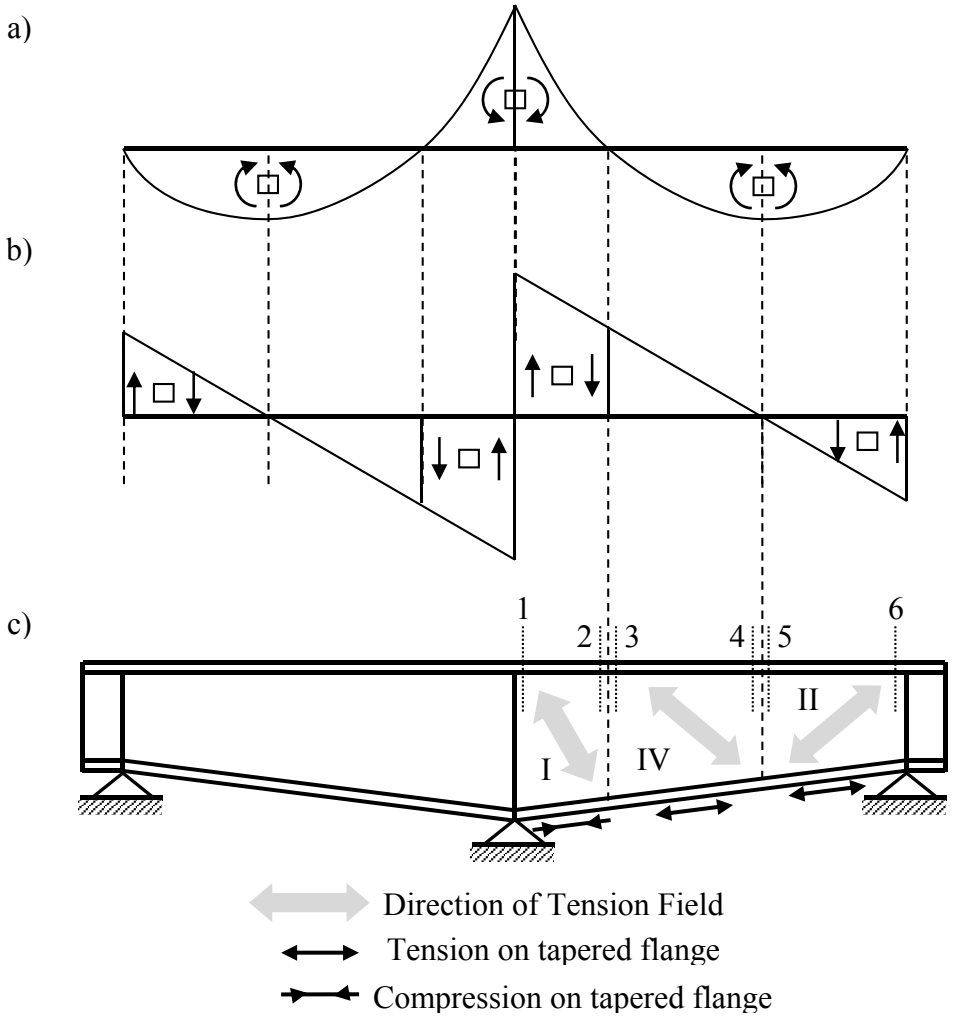

Figure 3 Classification of the web into different typologies; (a) bending moment diagram, (b) shear force diagram and (c) web typology

1.3. Goals and objectives

With the increasing utilization of tapered BGCWs worldwide [1], a better understanding of the true behaviour of such girders under shear loading becomes essential. Consequently, this thesis extends the paper by Hassanein and Kharoob [10] with respect to bridges of Case I and Case II.

Among the four typologies shown in Figure 3, Panels of Case I are the most common case which appears frequently near to the intermediate supports of continuous bridges; see the two examples presented in Figure 4. Accordingly, the objective of this thesis is to provide additional data to engineers and scientific community on the strength and behaviour of the tapered BGCWs of Case I and Case II under shear loads. As a result, the following new points (as suggested at the end of Ref. [10]) are added to literature for the first time:

1. The thesis defines the validity limit of the previously proposed design strength [10] for the tapered BGCWs regarding the initial imperfection proposed by eurocode 3 part 1-5 [12]. This was made by generating FE models with initial imperfections $h_{w1}/200$
2. Models with λ_s greater than 0.6 (belonging to the second part of Eq. (1)) using the limiting initial imperfections, as proposed from the previous point, are generated to check the proposed design equation.

3. The thesis investigates the effect of the aspect ratio of the web panel (a/h_{w1}) on the shear strength of the tapered BGCWs.

4. The thesis expands the pool of available results by considering tapered BGCWs with different inclination angles ($\gamma\circ$).

5. Finally, the thesis checks the proposed design model [10] using these additional parametric study results as well as the full slenderness parameter range (greater than 0.6).

(a) Kurobegawa Bridge (b) Ohmi-Ohdori bridge

Figure 4 Linearly tapered bridge girders with corrugated webs of Case I

Chapter 2. State of the Art.

2.1. Introduction

In steel and composite construction, is quite frequent to find us with design situations of structural systems where the stresses which it acts on specific girder area are great magnitude and they vary at directrix of element. In such situations, the use of tapered girders provide an economic and efficient solution.

In this chapter, it presents the theory background about steel plate shear buckling behaviour and how to get critical shear buckling stress.

Also, it exposes relevant points about post-critic shear buckling behaviour of BGCWs undergo internal shear force. In the same way, to provide a general vision from different researches who developed models to predict ultimate shear stress.

2.2. Behaviour of plate girders.

It can recognize two stage. First stage, it can see a lineal response, while in the second phase appears non lineal phenomenon. In the lineal stage, Navier-Bernoulli hypothesis applies, to get a lineal distribution of normal stress over cross-sectional girder. This occur to small values of bending moments.

Non lineal stage is get when the stress that acting on the girder overcomes yield strength material or when to appear local instability on plate that form part of girder. In this stage, the Navier-Bernoulli hypothesis no longer met.

2.2.1. Lineal Behaviour of plate girders

On cross sectional area of plate girder, among lineal stage, it induces normal stress and shear stress owing to bending moment.

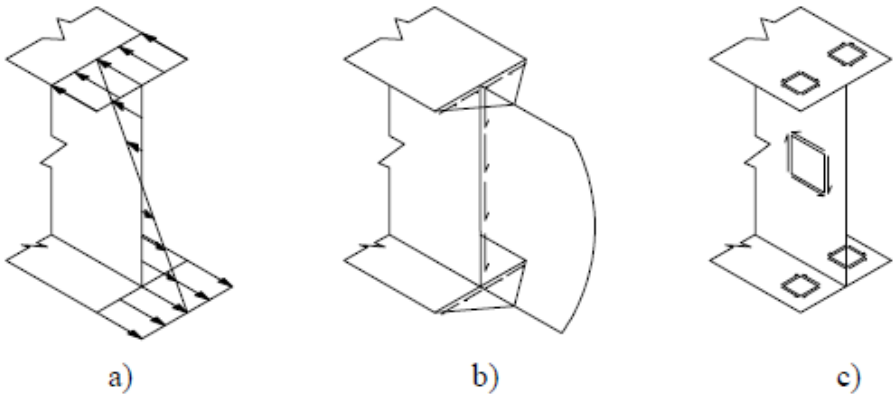

Figure 5 Distribution of normal stress and shear stress of plate girders.

The flexural stiffness of plate girders is obtained, by defining the geometry of flanges and the distance between them. The flanges are design to resist the axial force generated from the bending. In the other hand, the web give the shear resistance, as can be seen in figure 5.b. As plate girder should have lower self-weigh as possible, the thickness web can reduce it, as long

as, it guarantees that the web is able to resist the shear stress which they are generated in its contour.

Owing to the web panel which is subjected shear stress state in its contour, such panel can be slender, and its behaviour can be interpreted as a slender panel undergo shear stress in its contour, due such panel experiments a shear stress increase process, its behaviour is lineal until for specific value of shear stress, the panel suffer normal displacement to its mid-plane.
The value of the shear stress for which the shear buckling occurs, it is known as critical shear buckling stress.

Critical shear buckling stress of thin plate.

In order to meet the different factors and variables involved in the instability from web panel of girder, it explores the mathematical resolution for the calculation of the critical shear buckling stress of thin plates undergo shear stresses.

The approach which to allow determining the critical shear stress of web panel focuses towards the study of thin plate subjected to a uniform distribution of shear stress, where the boundary conditions are those for simply supported edge. The behaviour of the web panel will therefore be a thin plate undergo shear strength.

The interpretation of the web panel as a simply supported plate subjected to a uniform distribution of shear stress on the edges, it is an estimate to the actual situation. Owing to the fact that along the edge of the web the shear stress distribution is parabolic (see figure 5.b). However, consider such plate with a uniform distribution of shear stress helps the obtaining of a mathematical solution for the calculation of the critical shear buckling stress.

The critical shear buckling stress of thin plates was at first studied by Boobnoff and Timoshenko (Bleich, 1952). Boobnoff studied the problem of the instability of a rectangular plate simply supported subject to states of flexural stress and compression stress. In such studies, the hypothesis that stresses act in the mid plane of the plate was take in account. Timoshenko got a practical solution to this problem.

Timoshenko got analytical expressions for obtaining the critical shear buckling stress of thin plates with boundary conditions of simply supported edge. Such expressions were developed for flexural and compression stress states. Also, he extended his investigations in the case of plates undergo shear stress.

Next to the theoretical investigations carried out by Timoshenko, it carried out experimental tests in plate girders. Such tests had the purpose of verifying the expressions proposed by Timoshenko, in this way, to confirm if the behaviour of web panel of plate girders could be interpreted through the classical theory of plates. It is worth pointing that the experimental tests were carried out with the aim of knowing the behaviour from plate girders, beyond the instability of the web panel (post critical resistance).

Mathematical model proposed by Tymoshenko. Classical theory

The mathematical model which allows to determine the critical shear stress of rectangular plate part of the following hypotheses. A rectangular plate with boundary conditions of edges simply supported and undergo a state of shear stress in the mid-plane, as can be seen in figure 6.

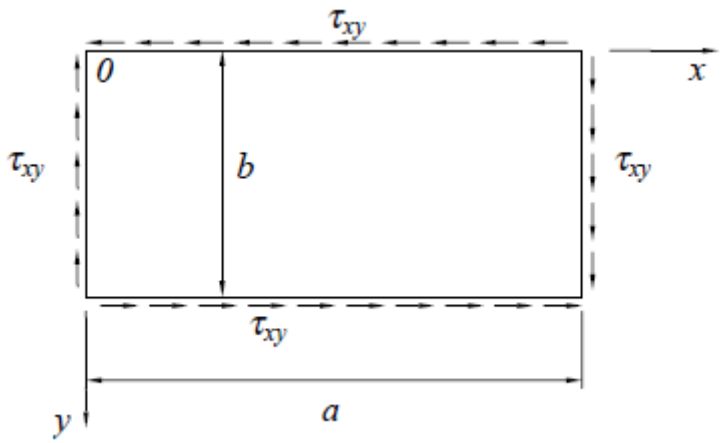

Figure 6 Rectangular Plate with conditions of edges simply supported and subject to state of shear stress.

The geometric parameters which define the plate are the length "a" of the plate, it defined by the distance among transverse stiffeners, depth web panel "b" and thickness t. The structural response of the plate can be obtained through the resolution of the differential equation of Saint Venant.

$$\frac{EI}{1-\nu^2}\left(\frac{\partial^4\omega}{\partial x^4}+2\frac{\partial^4\omega}{\partial x^2\partial y^2}+\frac{\partial^4\omega}{\partial y^4}\right)+t\cdot\left(\sigma_x\frac{\partial^2\omega}{\partial x^2}+\sigma_y\frac{\partial^2\omega}{\partial y^2}+2\tau_{xy}\frac{\partial^2\omega}{\partial x\partial y}\right)=0 \qquad (2)$$

Equation (2) was resolved by Timoshenko through the theorem of the stationary energy potential. This has allowed to determine analytical expressions for the estimate of the critical shear buckling stress for plates.

On the other hand, the method of stationary energy potential is used with success in those problems in which it is not necessary to obtain an exact solution rigorously, such as the case of web panel of plate girders; where is required to find a practical solution that allowed to calculate an estimated value for the critical shear buckling load.

However, this method is apply only to those cases where the deformed shape of the plate can be approximated by a function which fulfils the contour conditions, and achieve better results as soon as the function is approximates to deformed shape of shear buckled plate.

Wether a state of shear stress acts in the mid-plane of the plate; after each stress increase, small vertical displacements occur perpendicular to the mid-plane of the plate. If the work done by external forces is less than the flexural energy from the plate, for any deformed shape configuration, the plate will be stable.

However, if the work done by external forces is greater than the flexural energy from the plate, for any deformed shape, the plate will be unstable, therefore, it appears the shear buckling. Thus, it designating to V to the flexural energy when the plate shear buckles and U_ω to the potential energy of external forces, in accordance with the theorem of the stationary energy potential, it has:

$$V + U_w = stacionary \tag{2}$$

The flexural energy of the plate "V" is given by the expression:

$$V = \frac{D}{2}\int_0^a\int_0^b \left\{ \left(\frac{\partial^2\omega}{\partial x^2} + \frac{\partial^2\omega}{\partial y^2} \right)^2 - 2(1-\nu)\left(\frac{\partial^2\omega}{\partial x^2}\frac{\partial^2\omega}{\partial y^2} - \left(\frac{\partial^2\omega}{\partial x \partial y} \right)^2 \right) \right\} dxdy = 0 \tag{3}$$

While the change of potential energy Uω, is defined as the negative value of the work done by a uniform distribution of shear stress in the plate, which can be expressed as follows:

$$U_\omega = -\tau_{xy} t \int_0^a\int_0^b \frac{\partial\omega}{\partial x}\frac{\partial\omega}{\partial y} dxdy \tag{4}$$

In the moment in which takes place on the bifurcation of equilibrium (τ_{xy} will be critical shear buckling stress) undergo a small disturbance, in which the plate does not gain or loses energy, it must verify that V = Uω.

Thus, it is possible to define the function of the deformed shape of the mid-plane from the plate through the Fourier series.

$$\omega = \sum_{i=1}^{n}\sum_{j=1}^{n} f_{ij}\, sen\frac{i\pi x}{a}\, sen\frac{j\pi x}{b} \tag{5}$$

Thus, by limiting the number of terms from Fourier series to n=2 and defining the parameter of the plate form α=a/b, take in account the equation 5 in the expressions 2, 3 and 4, to allow getting the calculus expression of critical shear buckling stress.

$$\tau_{cr} = \frac{\pi^2 E}{12(1-\nu^2)}\left(\frac{t}{b} \right)^2 k \tag{6}$$

Where "k" is the critical shear buckling coefficient, which depends on the shape of plate α. This parameter is determined by the following expression.

$$k = \frac{9\pi^2}{32}\frac{(1+\alpha^2)^2}{\alpha^3} \tag{7}$$

The value of k obtained with this expression, for α = 1, presents an error of approximately 15% the actual value. That error is increased to values from α > 1. This is due to the fact that in the procedure adopted have been used only two terms in the Fourier series (n = 2).
Therefore, It will be much better the approximation of "k" using a greater number of terms for n in the expression (5), Timoshenko got for several form parameters α, the corresponding values of critical shear buckling coefficients k (α < 2.5).

Thus, Skan and Southwell, through many research, obtained the value k = 5.34 for α = ∞. Also, Seydel obtained the value of k = 9.34 for α = 1. Likewise, Stein and Neff got values of "k" for several parameters of shape (Bleich, 1952).

2.2.2. Post critical behaviour of plate girders

The behaviour of rectangular steel plates subjected to shear load was deeply studied during last century and different theories were developed in order to describe and analyse the mechanisms that take place during the post-buckling state and finally, to determine their ultimate shear capacity.

Some of them were taken as a reference and evolved in time and other ones were implemented in design codes. The most important methods to be mentioned are: Basler's model (1960), Chern and Ostapenko (1969), the Rotated Stress Field Model developed by Höglund (1971, 1997) and Tension Field Model developed in Cardiff and Prague by Porter et al. (1975) and Rockey and Škaloud (1972).

In most cases, the models are based on the assumption of simply supported rectangular plate and do not consider actual boundary conditions existing in the flange–web junctions and in the stiffener–web junctions neither the geometry of the tapered steel plate girder. In the last years, some researchers, among others Lee et al. (1996), Mirambell and Zárate (2000), Estrada et al. (2008) have demonstrated the importance of these effects.

Almost all ultimate shear strength models for tapered plate girders proposed in literature are based on the previous presented models for rectangular plate girders. Several models for tapered girders have been developed by: Falby and Lee (1976), Davies and Mandal (1979), Takeda and Mikami (1987), Roberts and Newmark (1997), Zárate and Mirambell (2004) and Shanmugam and Min (2007). Recently, some other numerical studies have been published by Abu-Hamd M. and Abu-Hamd I. (2011).

Here, also it is important to point out that all above-mentioned models demonstrate various limitations. In this way, the model presented by Falby and Lee based on the Basler's theory assumes that for tapered plate girders with significant angle of the inclined flange, the critical shear load may be calculated according to the classic theory as for simple supported rectangular plates, but using the average depth of the trapezoidal panel.

This method seems to give more realistic results for the ultimate shear resistance of tapered members compared to those ones obtained according to the theory for rectangular plates, however it does not take into account the contribution from the flanges in resisting the shear load.

In the method developed by Davies and Mandal for tapered plate girders, the simplified truss model loaded within the tip was used. This model assumes that the ultimate shear capacity may be calculated as a superposition of two tensional states: buckling and post-critical shear reserve.

However the critical shear load is calculated in the same way like it was proposed by Falby and Lee, the model takes into account the contribution from the flanges and the so called Resal effect and generally gave satisfactory results.

On the other hand, the researchers admitted that all tested cases were conducted for a small range of the geometric parameters and with the same slope of the inclined flange, so it was

recommended to verify the model with experimental tests conducted for various geometries of tapered panels.

The next model for assessment the ultimate shear resistance of tapered plate girders was proposed by Takeda and Mikami and based on the Chern's and Ostapenko's theory for prismatic members. Also this approach assumes the ultimate shear resistance as a superposition of the pre-critical and post-critical states.

The difference comparing to the previously mentioned methods is in assessment of the critical shear load. In this case the critical stress is calculated with use of formulae derived from Finite Element Theory applied to instability analysis of trapezoidal plates. Also this model discards contribution from the flanges in carrying the shear force what is opposite to the hypothesis stated before by Davies and Mandal.

Some experimental tests on tapered aluminium girders conducted by Roberts and Newmark (1997) allow them to observe that collapse mechanisms of tapered steel and aluminium girders are drastically different and existing theories for steel plates cannot be copied and adopted in easy way for aluminium.

Also last decade brought several attempts of solving the problem of the ultimate shear resistance of tapered steel plate girders. One of them was proposed by Zárate and Mirambell (2004). The method takes into account actual boundary conditions and trapezoidal shape of tapered plate girders in both pre-buckling and post-buckling phases.

The proposal is based on the Tension Field Method and on the results obtained from numerical studies conducted with use of Finite Element Method. In order to obtain the ultimate shear resistance the iterative process has to be carried out.

However the analytical model is valid for various geometric parameters of tapered panel and offers a very good approach for non-prismatic members; it can be used only for one of four possible structural situations where the tension field is developed on the shortest diagonal of the web-panel and the inclined flange is under compression. A new element introduced in this method is the consideration of the influence of the Resal effect.

Apart from the several above-mentioned approaches to assess the ultimate shear resistance of tapered steel plate girders, there are no specific rules for tapered plate girders in current codes.

For calculating ultimate strength of such members, EN 1993-1-5 suggests to use the expressions for prismatic plates without any changes if the angle of the inclined flange is not greater than 10º.

In other cases, it is recommended to calculate a tapered plate as a rectangular one with its larger depth. Unfortunately, this method cannot be used for some cases of tapered panels because overestimates the ultimate strength and thereby does not satisfy the safety requirements.

2.3. Prismatic plate girders with corrugated web.

Girders with steel corrugated webs has been used as structural members in Bridges. A trapezoidally corrugated web is composed of a series of longitudinal and inclines panels, as can be seen from Figure 6.

Owing to out-of-plane stiffness, corrugated web panels have much higher buckling strength compared with flat panels. Therefore, the use of stiffeners is not necessary by using them as bridge girder web and the required web thickness is reduced [10].

2.3.1. Elastic shear buckling behaviour of corrugated webs

In the following, a brief discussion about the three buckling modes of the corrugated webs (local, global and interactive modes) is provided.

Local shear buckling

Local buckling, as can be seen in Figure 8.a. is controlled by the slenderness of the individual folds of the web. It occurs when a flat subplate or fold between vertical edges has a large width-to-thickness ratio. In this mode, the corrugated web acts as a series of flat plate sub-panels that mutually support each other along their vertical edges and are supported by the flanges at their shorter horizontal edges.

The elastic local shear buckling stress of the corrugated webs $\tau_{cr,L}$ can be determined by the classical plate buckling theory, as be indicated in equation 9.

Global shear buckling

Figure 8.b. represents the global buckling mode. When global buckling controls the failure mode, the buckling stress can be calculated for the whole corrugated web panel, using the orthotropic-plate buckling theory; refer to Galambos [16].

However, the calculation of the global elastic buckling stress ($\tau_{cr,G}$) for the corrugated webs has been initiated by Easley [17], as be indicated in equation 10.

Interactive shear buckling

These shear buckling modes termed as interactive buckling, which can be seen in Figure 8.c, are explained as a result of the interaction between local and global buckling. Interaction formulae originally proposed by Lindner and Aschinger [18] are generalized as follows:

$$\tau_{cr,I} = \frac{\tau_{cr,L} \cdot \tau_{cr,G}}{\left(\left(\tau_{cr,L}\right)^n + \left(\tau_{cr,G}\right)^n \right)^{\frac{1}{n}}} \tag{8}$$

Where $\tau_{cr,L}$ is the local shear buckling stress, $\tau_{cr,G}$ is the global shear stress, both are calculated from the following equations:

$$\tau_{cr,L} = k_L \frac{\pi^2 E}{12(1-\nu^2)} \left(\frac{t_w}{w}\right)^2 \tag{9}$$

$$\tau_{cr,G} = k_G \frac{D_x^{0.25} D_y^{0.75}}{t_w h_w^2} \tag{10}$$

Where E is the Young's modulus of elasticity, ν is the Poisson's ratio, w is the maximum fold width (maximum of flat panel width b and inclined panel width c as shown in Figure. 5), t_w is the web thickness, k_L is the local shear buckling coefficient and k_G is the global buckling coefficient.

k_L is the local shear buckling coefficient which is a function of the aspect ratio of the sub-panel (w/hw), as follows:

$$k_L = 5.34 + 4\left(\frac{w}{h_w}\right)^2 \tag{11}$$

k_G is the global buckling coefficient. Elgaaly et al. [19] assumes that the web is relatively long compared to hw and suggest that k_G is to be taken as 31.6 (assuming the web is simply supported by the flanges) or 59.2 (assuming that the flanges provide the web with fixed supports). Easely [17], however, suggests that k_G varies between 36 and 68.4.

The transverse bending stiffness per unit length of the corrugated web (D_x), the longitudinal bending stiffness per unit length of the corrugated web (D_y) and I_y are defined as:

$$D_x = \frac{q}{s} \cdot \frac{E t_w^3}{12} \tag{12}$$

$$D_y = \frac{E I_y}{q} \tag{13}$$

$$I_y = 2bt_w\left(\frac{h_r}{2}\right)^2 + \frac{t_w h_r^3}{6\sin\alpha} \tag{14}$$

It is worth pointing out that w, is the bigger of b and c, this parameters are used in equation (9)-(14).

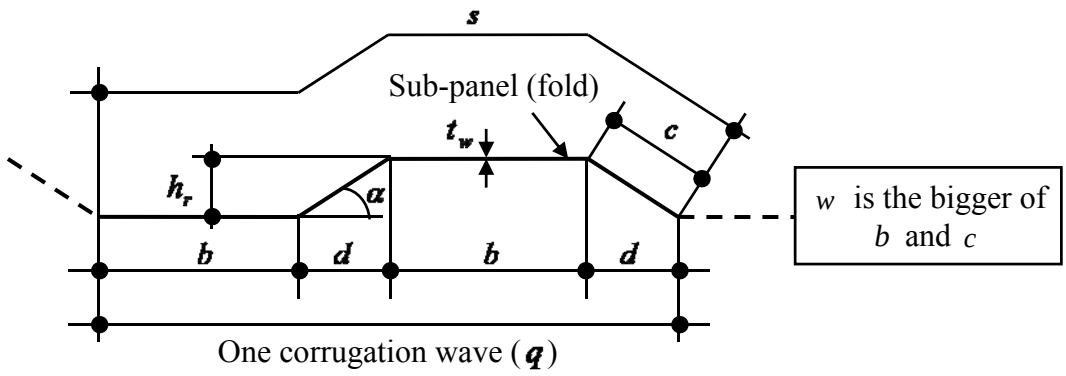

Figure 7 Corrugation configuration and geometric notation.

However, several derivations from Eqs. (10), (12), (13) y (14) for the calculation of the global shear buckling stress were made by other researchers. For example, Abbas [20] expressed the global shear buckling stress directly in terms of the geometric parameters of the trapezoidal corrugations. Another expression for $\tau_{cr,G}$ based also on Eqs. (10), (12), (13) y (14) was provided by Yi et al. [2]. A survey for these methods for more details can be found in [21].

a)

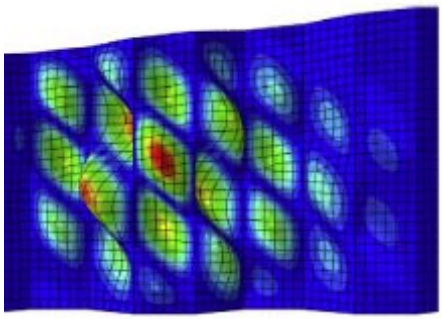

b)

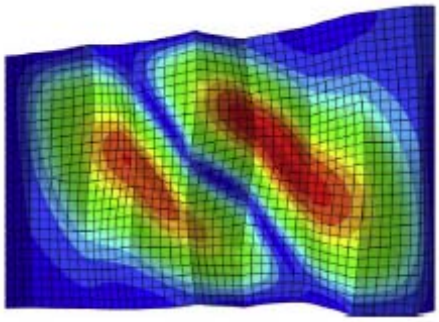

c)

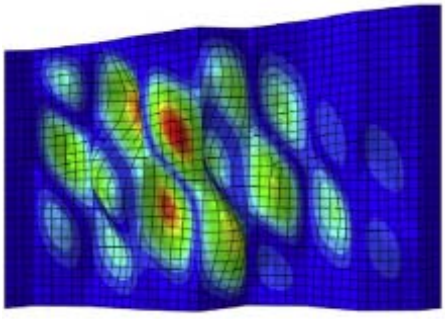

Figure 8 Local (a), global (b) and Interactive (c) shear buckling mode**.**

This buckling mode represents the specific mode from current parametric study, and it is base to carry out nonlinear analyses.

2.3.2. Design shear strength in the literature and available experimental full-scale tests

The normalized experimental shear strengths (τ_e/τ_y) of the fullscale BGCWs conducted in [3,8,22] were compared to the available design formulae according to [3,8,21]. A brief description for these shear design formulae is provided in the following paragraphs, using the geometric notations provided in Figure 7.

It should be mentioned that the details of these experiments can be found in [21] without reporting the details of the flanges of the bridges. The corrugation details of the tests are given in Table 1. However, another nine bridge girders tested by Gil et al. [22] were also used to check the validity of available design shear strengths.

Girder	b (mm)	d(mm)	tw(mm)	hw(mm)	α^o	$\tau e/\tau y$
G7A[8]	300	200	6.3	1500	36.9	0.91
G8A[8]	300	200	6.27	1500	36.9	0.85
M12[5]	250	220	4	2000	17.18	0.64
M13[5]	220	180	4	2000	14.63	0.62
M14[5]	220	180	4	2000	18.72	0.77
L1[23]	450	300	4.8	1500	33.7	0.72
L2[23]	550	300	4.8	1500	32.2	0.6
L3[23]	450	300	4.8	1500	9.4	0.51
L4[23]	550	300	4.8	1500	10.6	0.46
I1[23]	320	100	4.8	2000	24	0.95
I2[23]	350	100	3.8	2000	16	0.52
G1[23]	200	180	4.8	2000	14.2	0.79
G2[23]	160	50	3.8	2000	33.4	0.83
G3[23]	160	100	3.8	2000	15.1	0.85

Table 1 Profiles of available test for BGCWs [3, 8, 22]

Design shear buckling strength ($\tau_{n,M}$) according to Moon et al.[3]

To calculate the shear buckling strength ($\tau_{n,M}$) according to Moon et al. [3], the shear buckling parameter of corrugated webs (λ_s) should firstly be calculated along with Eq. (15).

The interactive shear buckling coefficient (k_I) is then to be calculated as defined in Eq. (16), which takes into consideration the lower bound values of the local (k_L) and global (k_G) buckling factors; 5.34 and 36, respectively.

The shear strength of corrugated webs can then be determined directly using Eq. (1) which adopts a buckling curve from the design manual for PC bridges with corrugated steel webs [24]. It should be noted that to calculate the shear buckling strengths according to Moon et al. [3] no need to calculate the local and global shear buckling strengths. This shear buckling strength ($\tau_{cr,M}$) is based upon the 1st-order interactive buckling strength proposed by Yi et al. [2].

$$\lambda_s = 1.05\sqrt{\frac{\tau_y}{k_I E}}\left(\frac{h_W}{t_w}\right) \tag{15}$$

$$k_I = \frac{30.54}{5.34\left(h_r / t_w\right)^{-1.5} + 5.72\left(w / h_w\right)^2} \tag{16}$$

Design shear buckling strength ($\tau_{n,D}$) according to Driver et al.[8]

Equation (17) for the nominal shear strength ($\tau_{n,D}$) according to Driver et al. [8] was proposed for the use in the design of BGCWs. This equation considers the effects of both local and global buckling in a single interaction formula. It was suggested to be applied over the full range of behavior, including cases where inelastic buckling and yielding controls.

$$\tau_{n,D} = \sqrt{\frac{\left(\tau_{cr,L} \cdot \tau_{cr,G}\right)^2}{\left(\tau_{cr,L}\right)^2 + \left(\cdot\tau_{cr,G}\right)^2}} \tag{17}$$

The elastic local shear buckling stress is provided in Eq. (9), while the global shear buckling stress as adopted from Abbas [20] is:

$$\tau_{cr,G} = k_G F\left(\alpha,\beta\right)\frac{E t_w^{0.5} b^{1.5}}{12 h_w^2} \tag{18}$$

Where k_G is the global buckling coefficient. Elgaaly et al. [19] assume that the web is relatively long compared to h_w and suggest that k_G is to be taken as 31.6 and 59.2 assuming simple and fixed web-flange boundary conditions, respectively. Easely [17], however, suggests that k_G varies between 36 and 68.4.

The lower bound values for the local (k_L) and global (k_G) buckling factors according to Driver et al. [8] are as well recommended; 5.34 and 31.6, respectively. F(α,β) is a coefficient based on the web corrugation geometry as follows:

$$F\left(\alpha,\beta\right) = \sqrt{\frac{(1+\beta)\sin^3\alpha}{\beta+\cos\alpha}} \cdot \left(\frac{3\beta+1}{\beta^2\left(\beta+1\right)}\right)^{0.75} \tag{19}$$

Where β is the ratio of b to c; and α is the corrugation angle. It should be noted that the values of $\tau_{cr,L}$ and $\tau_{cr,G}$ should not be greater than $0.8\tau_y$. Otherwise, inelastic shear buckling strength according to Elgaaly et al. [19] should be used.

Design shear buckling strength ($\tau_{n,S}$) according to Sause and Braxtan [21]

Recently, Sause and Braxtan [21] proposed Equation (20) for the design shear buckling strength ($\tau_{n,S}$).

$$\tau_{n,S} = \tau_y \left(\frac{1}{\left(\lambda_{I,3}\right)^6 + 2}\right)^{1/3} \tag{20}$$

Where $\lambda_{I,3}$ is the interactive slenderness parameter which can be calculated from Equation (20) with n = 3. The local (k_L) and global (k_G) slenderness parameters can be determined from

Equations (21) and (22). Note that the global (k_G) buckling factor is calculated by Sause and Braxtan [21] in line with Easely [17]; k_G varies between 36 and 68.4 for simple and fixed boundary conditions, respectively. The global shear buckling stress is to be calculated using Equation (18).

$$\lambda_{I,n} = \lambda_L \lambda_G \left(\left(\frac{1}{\lambda_L} \right)^{2n} + \left(\frac{1}{\lambda_G} \right)^{2n} \right)^{1/2n} \tag{21}$$

$$\lambda_L = \sqrt{\frac{12\left(1-\nu^2\right)\tau_Y}{k_L \pi^2 E}} \frac{w}{t_w} \tag{22}$$

$$\lambda_G = \sqrt{\frac{12 h_w^2 \tau_y}{k_G F(\alpha,\beta) E t_w^{0.5} b^{1.5}}} \tag{23}$$

It is worth pointing out that this design strength ($\tau_{n,S}$) was verified in [21] using a final test results of 22 tests. However, it was noticed that the web-depth (hw) of the girders is ranging from 298 mm to 2000 mm with an average of 606 mm.

This relatively small scale of tests (especially the web thicknesses (t_w) that were as small as 0.64 mm) almost had an influence on these shear test results.

Considerable differences in material stress–strain behavior, and the geometric imperfections and residual stresses induced by fabricating the web and welding the web to the flanges, should be expected between such thin sheet material and the plate material used in actual bridge girders [8]. Therefore, this group was not used in the comparison with design shear strength formulae because it cannot represent behavior of actual bridges.

Effects of Tapered Web Typology

It can be observed from [5] that the $\tau_{cr,FE}$ value becomes less than that of the prismatic web for Cases I and II, while it is higher for Cases III and IV. Hence, it could be concluded that the predictions of the τ_{cr} value for tapered webs based on prismatic web calculations may overestimate the stresses for Cases I and II, whereas it may provide highly conservative values for Cases III and IV.

By the analysis of the $\tau_{cr,FE}$ values of the corrugated webs, it was possible to connect them with the critical values of the prismatic webs ($\tau_{cr,FE,P}$). Accordingly, the following equations are proposed to predict the critical buckling stresses follow Hassanein et al [5].

$$\tau_{cr,\mathrm{Prop}} = \tau_{cr,FE,P} / (1 + \tan\gamma) \text{ - Case I} \tag{24}$$

$$\tau_{cr,\mathrm{Prop}} = 1.04\,\tau_{cr,FE,P} / (1 + \tan\gamma) \text{ - Case II} \tag{25}$$

$$\tau_{cr,\mathrm{Prop}} = \tau_{cr,FE,P} / (1 - \tan\gamma) \text{ - Case III} \tag{26}$$

$$\tau_{cr,\mathrm{Prop}} = 0.94\,\tau_{cr,FE,P} / (1 - \tan\gamma) \text{ - Case IV} \tag{27}$$

This equation will be useful to carry out the present analyses, take in account only Case I and Case II, both are the most found in the real bridges.

2.4. Tapered plate girders

In design structures, the engineer try to optimize the system structural. Therefore, it can get varying the resistant modulus and moment of inertia of cross-sectional area according to change over moment diagram, where inertia variation is obtained through the variation of the cross section depth and keeping horizontal upper flange panel.

The project and manufacture tapered plate girders was originally proposed for economic reasons, since it mean a savings in the consumption of the material. Subsequently, other benefits (such as the decrease of the weight of the structural system and obtaining a more slender appearance and a more aesthetic aspect of the structural system empowered their use.

In structural systems which in certain areas, there is a variation of the bending moment, as occur in areas close to intermediate supports of bridges. It will always be efficient from a structural point of view, to project span of tapered plate girders.

Probably, such a way to proceed will be both efficient as more unbalanced are the spans of the bridge. In the figure 1.b shows a clear example of the use of beams of inertia variable in metallic structures that must save important distances, as in the case of bridges. Tapered plate girders

2.4.1. Shear models for tapered plate girders

The behaviour of the rectangular steel plates subjected to shear load was deeply studied during last century and different theories were developed in order to describe and analyse the mechanisms that take place during the post-buckling state and finally, to determine their ultimate shear capacity.

Some of them are implemented in design codes: the Rotated Stress Field Model developed by Höglund (1971, 1997) and the Tension Field Model developed in Cardiff and Prague by Porter et al. (1975) and Rockey and Škaloud (1972).

However, these models are based on the assumption of simply supported rectangular plates and do not consider the boundary conditions existing in the flange–web junctions and in the stiffener–web junctions neither the geometry of the tapered steel plate girder. Some authors, among others Lee et al. (1996), Mirambell and Zárate (2000), Estrada et al. (2008) have demonstrated the importance of these effects.

The ultimate shear strength models for tapered plate girders proposed in literature are based on previous presented models for plate girders with constant depth. Several models for tapered girders have been developed by: Falby and Lee (1976), Davies and Mandal (1979), Takeda and Mikami (1987), Roberts and Newmark (1997), Zárate and Mirambell (2004) and Shanmugam and Min (2007). Recently, some other numerical studies have been published by Abu-Hamd and Abu-Hamd (2011).

Ultimate shear strength for tapered plate girders

It is well known that the structural behaviour of a prismatic steel plate girder subjected to an increasing shear load up to failure may be divided into three clearly different phases. Prior to buckling, equal tensile and compressive principal stresses are developed in the web panel. In the post-buckling stage, an inclined tensile membrane stress state is developed.

The total stress state is obtained by adding the post-buckling to that induced at buckling. Once the web has yielded, failure of the steel plate girder occurs when plastic hinges are formed in the flanges. The failure load can be determined from the consideration of the mechanism developed in the last stage (upper bound solution) or by the consideration of the equilibrium of forces (lower bound solution (Porter et al., 1975)).

The behaviour of a tapered steel plate girder subjected to increasing shear load is practically identical to that exhibited in a prismatic steel girder. When the web buckles under the action of direct stresses, it does not exhaust the full capacity of the plate.

After buckling, a significant increase in the strength of the steel plate girder can be observed. Experimental tests and numerical studies carried out on tapered steel plate girders reveal the existence of postcritical strength, by means of the development of the diagonal tension field anchored in the stiffeners and flanges.

Some models for the determination of the ultimate shear strength for tapered plate girders have been presented in the last years. All these studies are based on the tension field method, but one determines the ultimate shear load by the lower (equilibrium) bound method (Zárate and Mirambell, 2004); the other one by the upper (mechanism) bound method (Shanmugam and Min, 2007) and other one by both methods (Davies and Mandal, 1979).

It is important to explain here the limitation of the existing methods. The proposal of Zárate and Mirambell (2004) was thought only for these cases where the diagonal tension field develops in the short geometrical diagonal of the web panel.

On the other hand, although the models proposed in (Shanmugam and Min, 2007) distinguish two different design situations, where inclined flange is in tension or in compression, there is no difference about the direction of the tension field.

In order to evaluate the methods abovementioned, a numerical study for rectangular and tapered plate girders was conducted. Research included various geometrical parameters and both situations, where the inclined flange is subjected to tension or compression, were analysed in (Real et al., 2010).

The main conclusion of this study was that further ultimate shear models for tapered steel plate girders need to be developed in order to accurately evaluate the actual behaviour of tapered plate girders subjected to shear loads and their postbuckling resistance.

2.4.2. Shear resistance according to EN 1993-1-5

Despite being a very common type of beams, there are no specific rules for tapered plate girders in current codes. For calculating ultimate strength of tapered plate structures, EN 1993-1-5

suggests to use the expressions for prismatic plates without any changes if the angle of the inclined flange is not greater than 10°. In other cases is recommended to calculate a tapered plate as a rectangular plate with its larger depth. As it is shown in this paper, this approach cannot be used for some cases because overestimates the ultimate strength and thereby do not satisfy the safety requirements.

Chapter 3. Parametric studio of Bridge Girder Corrugated Webs (BGCWs)

3.1. Introduction

This document provides the behaviour of different web panels existing in linearly tapered Bridge Girders Corrugated Webs (BGCWs). It used two different types of web panels, one belongs to Dole Bridge and other one belongs to Maupre Bridge, as can be seen from figure 9.

Maupre Bridge is composed of prismatic girder corrugated web, on the other hand, Dole Bridge is composed of tapered parabolic Bridge Girders Corrugated Webs (BGCWs). Firstly, it should be investigate the behaviour of linearly tapered bridge girders, then it could be extended to tapered parabolic girders, such as it made in previously research of prismatic girders [5-6].

(a) Dole Bridge (b) Maupre Bridge

Figure 9 Bridge girders corrugated webs analysed herein. (a) Dole Bridge, (b) Maupre Bridge.

Following the nomenclature described in figure 7, in table 2, it find the dimensions of each wave depending the bridge.

BGCWs	b [mm]	d [mm]	c [mm]	q [mm]	s [mm]	hr [mm]	α°
Maupre Bridge	284.0	241.0	284.0	1050.0	1136.0	150.0	31.9
Dole Bridge	430.0	370.0	430.0	1600.0	1720.0	220.0	30.7

Table 2 Profile of corrugated steel web and geometric properties.

The purpose of this chapter is to provide some information on the shear buckling behaviour of such girders, so that direct correlation with the finite element work and theoretical analysis could be made.

3.2. Nomenclature

Roman Letters

a	shear span
b	width of horizontal fold
c	width of inclined fold
d	horizontal projection dimension of the inclined fold
Dx	transverse bending stiffness per unit length of the corrugated web
Dy	longitudinal bending stiffness per unit length of the corrugated web
E	Young's modulus of elasticity of the steel material
f_y	yield strength of the steel material
f_u	ultimate strength of the steel material
h_w	web depth
h_{wo}	minimum depth of tapered corrugated web
h_{w1}	maximum depth of tapered corrugated web
h_r	depth of the corrugation cross-section
I_y	moment of inertia of the corrugated web as presented in Eq. 14
k_G	global shear buckling coefficient
k_L	local shear buckling coefficient
n	order of interactive buckling strength
q	length of one corrugation wave in the horizontal projection
s	actual length of one corrugation wave
t_w	web thickness
t_f	flange thickness
V	vertical shear force of the girder
$V_{ul,FE}$	FE ultimate shear strength
w	maximum fold width (maximum of flat panel width b and inclined panel width c)

Greek Letters

α	inclination angle of the inclined fold
γ	inclination angle of the upper or lower flange of the tapered girder
λ_s	shear buckling parameter of the corrugated webs
τ	average shear stress
τ_{cr}	critical shear buckling stress
$\tau_{cr,L}$	local critical shear buckling stress
$\tau_{cr,G}$	global critical shear buckling stress
$\tau_{cr,FE}$	FE critical shear stress
$\tau_{cr,I}$	interactive critical shear buckling stress
$\tau_{cr,FE,P}$	FE critical shear buckling stress of the reference prismatic web
$\tau_{cr,Prop}$	proposed critical shear buckling stress
τ_y	shear yielding strength of the steel material

$\tau_{ul,FE}$ FE maximum shear stress values
$\tau_{ul,M}$ shear strength values according to Moon et al. [3]
$\tau_{ul,S}$ shear strength values according to Sause and Braxtan [21]
$\tau_{ul,Prop}$ currently proposed ultimate shear stress $\tau_{ul,M,mod}$
ν Poisson's ratio of the steel material

3.3. Finite element model

The finite element (FE) model presented by Hassenein et al. [10] was utilized in the current parametric study. The Dole Bridge and Maupre bridge corrugation dimensions were used in this paper to generate full-scale tapered BGCWs (Figure 10) loaded under mid-span concentrated loads.

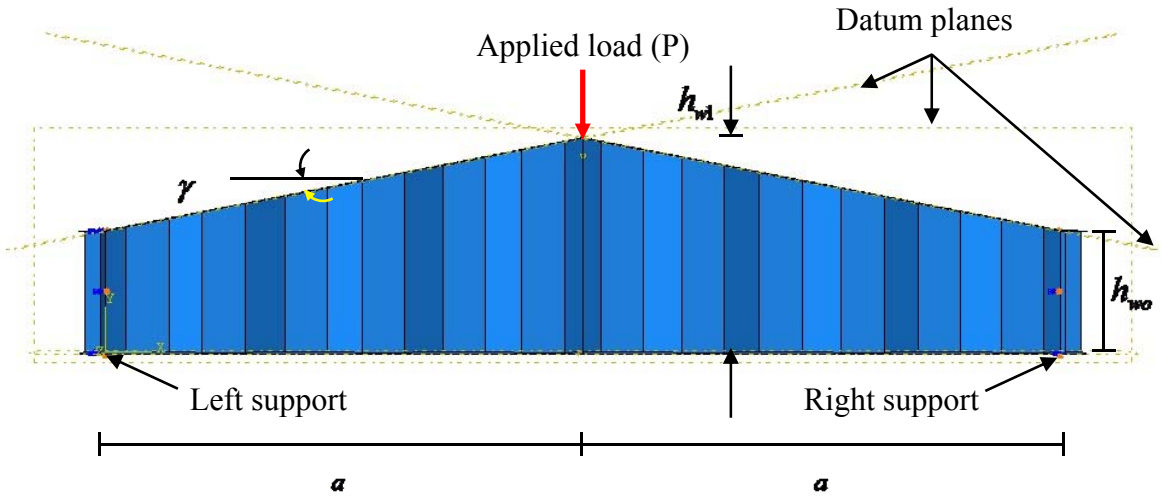

Figure 10 Full-scale tapered BGCWs.

To insure that the shear controls the failure modes of the tapered BGCWs, (1) the web thickness was chosen at range among 4 mm to 14 mm and (2) the loaded point was restrained laterally. Initial geometric imperfections, based on the first positive shear buckling mode, were included in the nonlinear analysis of the BGCW with values of $h_{w1}/200$[12].

The purpose of putting stiffeners on the girder was to help transfer the loads to web, this are dispose in the middle span and both end supports.

3.3.1. Finite element type and mesh

The loads were applied using the modified RIKS method. S8R5 reduced integration thin shell elements were employed to discretise the models in the current nonlinear analyses. Simply supported boundary conditions were applied to end sections.

In line with similar previous investigations [5,19,22], S8R5 reduced integration thin shell elements were employed to discretize the models in the current nonlinear analysis.

On the other hand, a convergence test in order to assess the requirement of the mesh refinement of the finite element discretization should be carried out especially for cases involving buckling.

Therefore, the girder was simulated four times. The difference between these models is the number of elements used across the width of each fold of the corrugation. As can be calculated from table 3, the difference in the results from the model with five and eight element is 1.15%.

Number of elements per fold	Failure Load [Kn]
5	818.7
6	824.4
8	828.3

Table 3 Effect of mesh size, girder model G109.

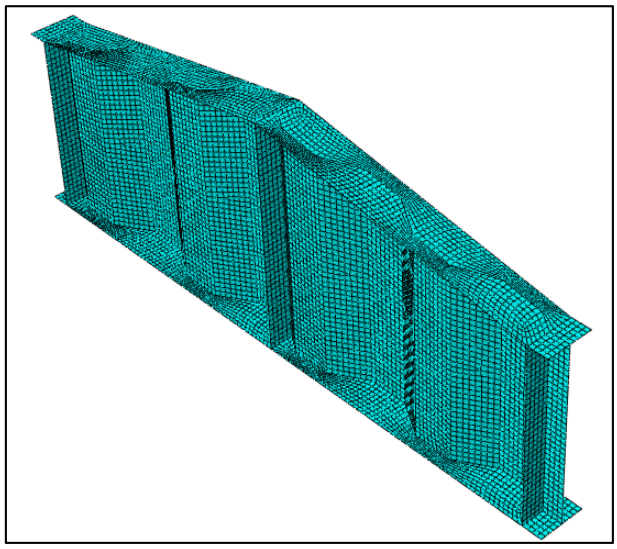

Figure 11 Mesh from current thesis from G109.

Hence, the computational effort without sacrificing the accuracy of the results, eight elements across each fold of the corrugation were employed in the current analysis. Figure 11 shows the shape of the current finite element mesh.

3.3.2. Material Properties

The displacement history was applied to the FE models along their mid-span web points at the intersection with lower flanges. A bilinear elastic-plastic stress-strain curve with linear strain hardening was used to simulate the steel material, as can be seen in figure 12.

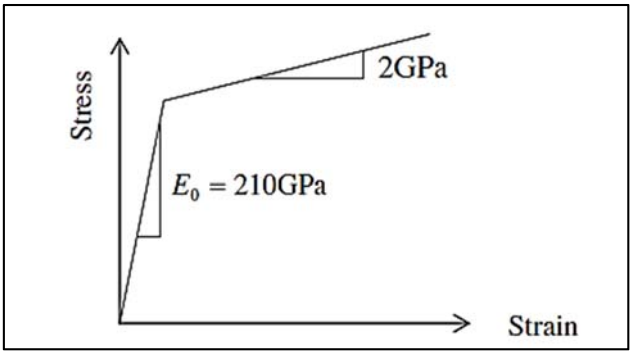

Figure 12 Steel material adopted model: bilinear stress-strain curve.

The steel material has been modelled as a von Mises material with isotropic hardening. The steel used was S355 according to EN 1993-1-1 [14], which has a yield (f_y) and an ultimate strength (f_u) of 355MPa and 510MPa, respectively.

3.3.3. Load application and boundary conditions

The bridge girder models considered herein are subjected to concentrated loads at their mid-spans, as can be seen in Figure 10, which ensure a constant shear force along them.

The load was applied in increments using the modified RIKS method available in the ABAQUS library [11]. In the RIKS method, the load is applied proportionally in several load steps. In each load step the equilibrium iteration is performed and the equilibrium path is tracked in the load–displacement space.

This method is often used in static analysis and shows to be a strong method for nonlinear analysis. The loads were applied as static uniform loads at the loaded point using displacement control. The non-linear geometry parameter (NLGEOM) was included to deal with the large displacement analysis.

As soon as boundary condition, simply supported boundary conditions were applied to end sections. At each end section, the twist rotation about x-axis of all nodes of the section was restrained (/$_x$ = 0.0).

The lateral displacement in z-axis of all nodes on the y-axis (at z = 0.0) was restrained (u_z = 0.0). The vertical displacement of the centre of the web was restrained (u_y = 0.0), while the longitudinal displacement in x-axis of a centre point at the lower flange was restrained (u_x = 0.0). In order to prevent flexural–torsional buckling (LTB) of the bridge girders. Lateral displacements were restrained at the loaded mid-span points.

3.3.4. Verification of Model

The results of five full-scale BGCWs having $tf / tw \geq 3$, which were tested experimentally by Moon et al. [3] and Driver et al. [8], are used herein to check the validity of available design shear strengths according to [3,8,21].

The literature describing experimental work on the shear behaviour of corrugated web girders does not report detailed measured values for initial imperfections. However, the FE model is verified herein through the simulation of specimen M12 which was tested experimentally by Moon et al. [3]. This is because they did not report the values of the initial imperfection for their other girders M13 and M14.

The geometric properties of girder M12 are provided in Table 1. Only the maximum measured initial imperfection of 17.9 mm was included in the model. However, this initial imperfection was found to concentrate near the compression flange of the girder.

In addition, the girder G7A tested by Driver et al. [8] was simulated using the dimensions given also in Table 1. The imperfection was found to be 4.06 mm in the fold just beside the applied load (fold 9).

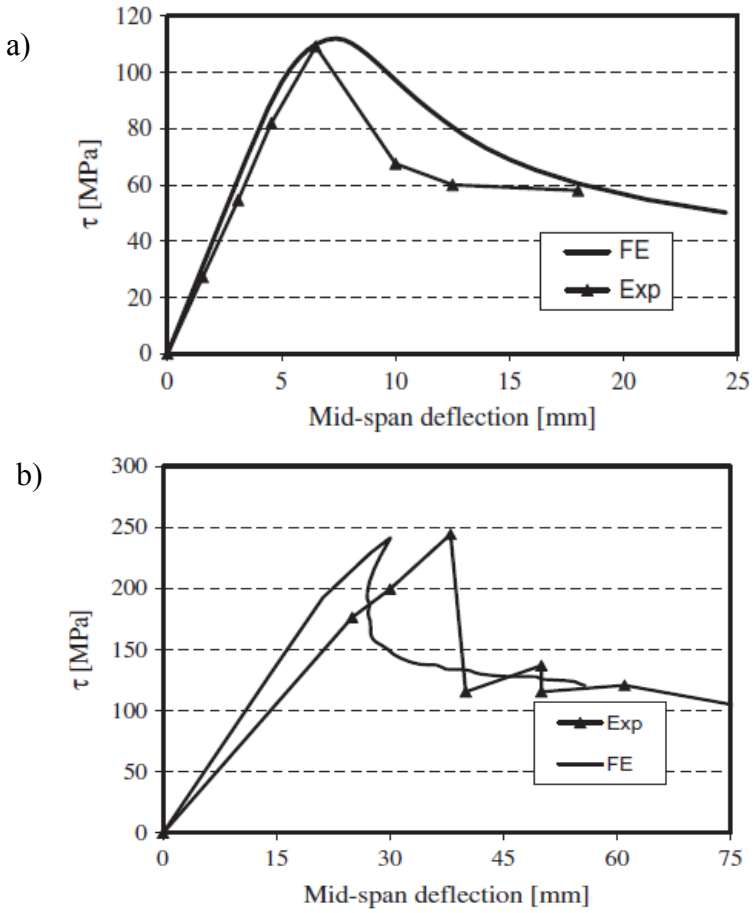

Figure 13 Shear stress versus mid-span deflection for specimen a) M12 [3] and b) G7A[8].

From the comparison shown in Figure. 13a and 13b, it can be noticed that the current modelling in almost reflects the real behaviour of the BGCWs. τ_{FE} / τ_y ratios for M12 and G7A are 1.03 and 0.99, respectively.

However, it is seen from Figure 13 that the experimental results follow the same trend but have somewhat lower strengths than the FE results. This difference for the case of M12 is attributed to the fact that the imperfection shape used in the finite element study, from the first eigenvalue analysis as proposed in [3], is different from that of the real girder.

Beside that the maximum measured initial imperfection concentrated near the compression flange of the girder, it is noticed that the girder M12 exhibits initial imperfection at the juncture of the corrugated web with the flanges, which is not the case for the finite element imperfection which is in the form of a sine wave without an imperfection at the web-flange juncture.

Also, the position of the maximum initial imperfection of girder G7A differs from that of the FE corresponding one. Hence, this could be considered as a verification for the current BGCWs. However, the current modelling is typical to the numerical modelling previously derived by other authors [6].

3.4. Input data

Three-dimensional FE models, using ABAQUS [11] FE package, were performed on one hundred sixty six tapered BGCWs covering the following parameters:

1. aspect ratio of the web panels (a/h_{w1}); (1.28, 1.92 and 2.56),
2. angle of the inclined flanges (γ); (10, 15, 20, 25˚), and
3. Thickness web (t_w); (4, 6, 8, 10, 12, and 14).

The flange width (b_f) was fixed to 500mm throughout the entire program. The webs of the girders were stiffened transversely at the supports and under the applied load. Out-standing plate stiffeners extending to the edge of the flanges of the plate girder were considered with a thickness of 25.4mm all through the thesis.

Unlike Hassanein and Kharoob [10] where almost of the models had shear buckling parameters (λ_s) less than 0.6, the values of λ_s of the current models were intentionally chosen to lay within second stage of the proposed design model; i.e. $0.6 < \lambda_s \leq \sqrt{2}$.

This was made to increase the range of the available data for the tapered BGCWs in literature, as can be seen in Table 3. This table shows the dimensions considered in this study. The table also contains the ultimate shear strength ($V_{ul,FE}$) of the girders beside the maximum shear stress ($\tau_{ul,FE}$) calculated with respect to the critical cross-section of the girders with the shorter depth (h_{wo}).

To ensure that all the tapered BGCWs failed by shear limit state away from the interaction with the flexural limit state by means of the development of flexural plastic hinges, the ratios between the ultimate and the plastic bending moments ($M_{ul,FE}/M_{pl}$) were computed and then added to Table 3, 4 and 5, it depends on the bridge and girder typology ; $M_{pl} = b_f t_f F_y (h_{w1} + t_f)$. From the table, it can be noticed that $M_{ul,FE}/M_{pl}$ ratios vary between 0.10 to 0.80 indicating that the flexural capacity limit state was still away to take place.

It is worth pointing out that herein it studies only two of four different typologies of tapered plate girders [9], as can be seen in figure 14:

I. Inclined flange in compression and diagonal tension field developed in the short diagonal.

II. Inclined flange in tension and diagonal tension field developed in the long diagonal;

(a) Case I:
Inclined flange under compression & tension field is developed in the short diagonal

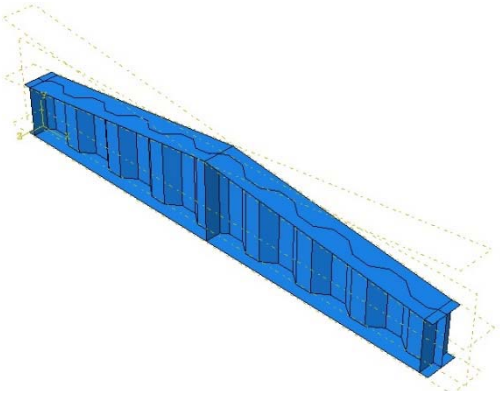

(b) Case II:
Inclined flange under tension & tension field is developed in the long diagonal

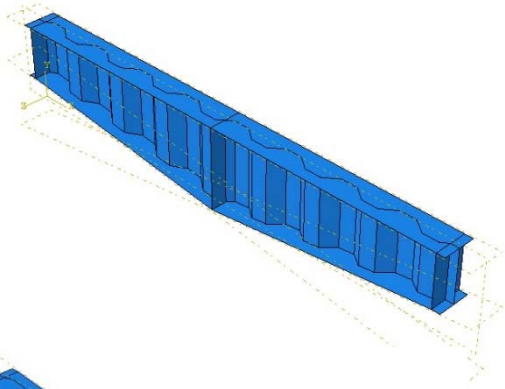

(c) Case III:
Inclined flange under compression & tension field is developed in the long diagonal

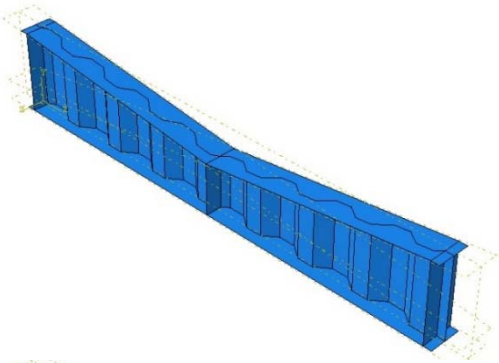

(d) Case IV:
Inclined flange under tension & tension field is developed in the short diagonal

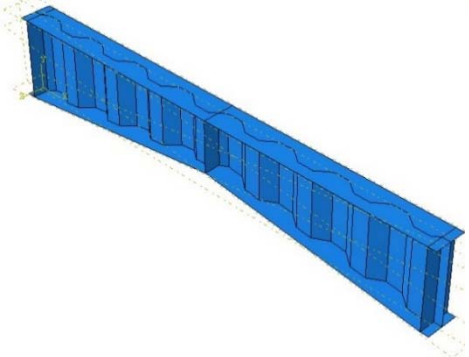

Figure 14 Types of tapered plate girders with corrugated webs.

It is well known that the amplitude and the shape of the initial web geometric imperfections play a significant role in the shear strength and behaviour of the girders with corrugated webs [3,8,13].

Accordingly, an initial imperfection amplitude equalling to the thickness of the corrugated web (t_w), as suggested by Driver et al. [8], was considered by Hassanein and Kharoob [10] to propose their design strength given herein by Equation 1, but herein, it will use $h_{w1}/200$ according to eurocode 1-3, anex D [12].

In table 4, 5 and 6 presents the results from nonlinear analysis. 54 girders has been analysed for every case, depend on profile Shape Bridge.

Girder	h_{wo} [mm]	h_{w1} [mm]	t_f [mm]	γ °	t_w [mm]	a [mm]	a/h_{w1}	λ_s	$\frac{M_{ul,FE}}{M_{pl}}$	$V_{ul,FE}$ [kN]	$\tau_{ul,FE}$ [MPa]
G1	1944	2500	50	10	4	3150	1.26	1.25	0.13	896.54	115
G2	1667			10	4	4725	1.89	1.25	0.17	817.86	123
G3	1389			10	4	6300	2.52	1.25	0.20	713.35	128
G4	1944			10	6	3150	1.26	0.91	0.24	1666.09	143
G5	1667			10	6	4725	1.89	0.91	0.30	1412.15	141
G6	1389			10	6	6300	2.52	0.91	0.37	1295.87	156
G7	1944			10	8	3150	1.26	0.75	0.38	2658.65	171
G8	1667			10	8	4725	1.89	0.75	0.48	2262.04	170
G9	1389			10	8	6300	2.52	0.75	0.54	1912.70	172
G10	1944			10	10	3150	1.26	0.65	0.55	3871.88	199
G11	1667			10	10	4725	1.89	0.65	0.65	3036.71	182
G12	1389			10	10	6300	2.52	0.65	0.72	2528.43	182
G13	1944			10	12	3150	1.26	0.59	0.79	5532.37	237
G14	1667			10	12	4725	1.89	0.59	0.91	4259.36	213
G15	1389			10	12	6300	2.52	0.59	1.00	3504.33	210
G16	1944			10	14	3150	1.26	0.54	0.83	5870.08	216
G17	1667			10	14	4725	1.89	0.54	1.08	5075.90	218
G18	1389			10	14	6300	2.52	0.54	1.05	3704.99	191
G19	1656			15	4	3150	1.26	1.30	0.12	870.25	131
G20	1233			15	4	4725	1.89	1.30	0.14	653.98	133
G21	811			15	4	6300	2.52	1.30	0.16	557.15	172
G22	1656			15	6	3150	1.26	0.95	0.20	1442.66	145
G23	1233			15	6	4725	1.89	0.95	0.25	1165.00	157
G24	811			15	6	6300	2.52	0.95	0.28	974.49	200
G25	1656			15	8	3150	1.26	0.78	0.31	2189.04	165
G26	1233			15	8	4725	1.89	0.78	0.37	1725.05	175
G27	811			15	8	6300	2.52	0.78	0.41	1440.93	222
G28	1656			15	10	3150	1.26	0.68	0.44	3122.37	189
G29	1233			15	10	4725	1.89	0.68	0.51	2399.83	195

G30	811			15	10	6300	2.52	0.68	0.49	1738.35	214
G31	1656			15	12	3150	1.26	0.61	0.62	4400.69	222
G32	1233			15	12	4725	1.89	0.61	0.63	2971.07	201
G33	811			15	12	6300	2.52	0.61	0.63	2202.47	226
G34	1656			15	14	3150	1.26	0.57	0.75	5310.65	229
G35	1233			15	14	4725	1.89	0.57	0.75	3539.13	205
G36	811			15	14	6300	2.52	0.57	0.84	2957.39	260
G37	1353			20	4	3150	1.26	1.35	0.11	788.34	146
G38	779			20	4	4725	1.89	1.35	0.13	587.90	189
G39	1353			20	6	3150	1.26	0.98	0.20	1424.90	176
G40	779			20	6	4725	1.89	0.98	0.22	1023.00	219
G41	1353			20	8	3150	1.26	0.81	0.30	2122.92	196
G42	779			20	8	4725	1.89	0.81	0.32	1514.16	243
G43	1353			20	10	3150	1.26	0.70	0.40	2782.69	206
G44	779			20	10	4725	1.89	0.70	0.32	1514.16	194
G45	1353			20	12	3150	1.26	0.64	0.51	3573.61	220
G46	779			20	12	4725	1.89	0.64	0.48	2267.02	242
G47	1353			20	14	3150	1.26	0.59	0.59	4174.79	220
G48	779			20	14	4725	1.89	0.59	0.63	2965.92	272
G49	1030			25	4	3150	1.26	1.40	0.10	672.27	163
G50	1030			25	6	3150	1.26	1.02	0.16	1136.19	184
G51	1030			25	8	3150	1.26	0.84	0.23	1649.19	200
G52	1030			25	10	3150	1.26	0.73	0.45	3167.68	307
G53	1030			25	12	3150	1.26	0.66	0.41	2884.97	233
G54	1030			25	14	3150	1.26	0.61	0.50	3555.35	246

Table 4 Full details of the current tapered BGCWs - Case I from Maupre Bridge

Girder	h_{wo} [mm]	h_{w1} [mm]	t_f [mm]	γ°	t_w [mm]	a [mm]	a/h_{w1}	λ_s	$\frac{M_{ul,FE}}{M_{pl}}$	$V_{ul,FE}$ [kN]	$\tau_{ul,FE}$ [MPa]
G55	1944			10	4	3150	1.26	1.23	0.17	1219.41	157
G56	1667			10	4	4725	1.89	1.23	0.18	841.06	126
G57	1389			10	4	6300	2.52	1.23	0.22	779.02	140
G58	1944			10	6	3150	1.26	0.90	0.25	1777.55	152
G59	1667	2500	50	10	6	4725	1.89	0.90	0.33	1531.81	153
G60	1389			10	6	6300	2.52	0.90	0.39	1376.55	165
G61	1944			10	8	3150	1.26	0.74	0.42	2980.40	192
G62	1667			10	8	4725	1.89	0.74	0.51	2376.33	178
G63	1389			10	8	6300	2.52	0.74	0.56	1981.78	178
G64	1944			10	10	3150	1.26	0.64	0.57	4027.92	207

G65	1667			10	10	4725	1.89	0.64	0.73	3449.99	207
G66	1389			10	10	6300	2.52	0.64	0.77	2714.91	196
G67	1944			10	12	3150	1.26	0.60	0.71	4979.58	213
G68	1667			10	12	4725	1.89	0.58	0.93	4350.96	218
G69	1389			10	12	6300	2.52	0.58	1.03	3621.81	217
G70	1944			10	14	3150	1.26	0.55	0.86	6040.45	222
G71	1667			10	14	4725	1.89	0.55	1.10	5149.15	221
G72	1389			10	14	6300	2.52	0.55	1.07	3771.23	194
G73	1656			15	4	3150	1.26	1.29	0.13	915.71	138
G74	1233			15	4	4725	1.89	1.29	0.15	726.83	147
G75	811			15	4	6300	2.52	1.29	0.18	626.95	193
G76	1656			15	6	3150	1.26	0.95	0.25	1751.12	176
G77	1233			15	6	4725	1.89	0.95	0.27	1274.54	172
G78	811			15	6	6300	2.52	0.95	0.31	1081.87	222
G79	1656			15	8	3150	1.26	0.78	0.35	2441.63	184
G80	1233			15	8	4725	1.89	0.78	0.40	1866.82	189
G81	811			15	8	6300	2.52	0.78	0.44	1556.33	240
G82	1656			15	10	3150	1.26	0.69	0.49	3483.00	210
G83	1233			15	10	4725	1.89	0.69	0.54	2537.05	206
G84	811			15	10	6300	2.52	0.69	0.65	2281.81	281
G85	1656			15	12	3150	1.26	0.62	0.63	4444.62	224
G86	1233			15	12	4725	1.89	0.62	0.71	3323.32	225
G87	811			15	12	6300	2.52	0.62	0.68	2400.38	247
G88	1656			15	14	3150	1.26	0.58	0.74	5235.20	226
G89	1233			15	14	4725	1.89	0.58	0.90	4236.41	245
G90	811			15	14	6300	2.52	0.58	0.91	3217.32	283
G91	1353			20	4	3150	1.26	1.34	0.12	816.07	151
G92	779			20	4	4725	1.89	1.34	0.14	644.28	207
G93	1353			20	6	3150	1.26	0.99	0.19	1371.42	169
G94	779			20	6	4725	1.89	0.99	0.25	1170.87	250
G95	1353			20	8	3150	1.26	0.81	0.30	2145.62	198
G96	779			20	8	4725	1.89	0.81	0.36	1690.03	271
G97	1353			20	10	3150	1.26	0.71	0.42	2946.31	218
G98	779			20	10	4725	1.89	0.71	0.48	2244.04	288
G99	1353			20	12	3150	1.26	0.64	0.54	3778.09	233
G100	779			20	12	4725	1.89	0.64	0.60	2819.74	301
G101	1353			20	14	3150	1.26	0.60	0.67	4686.87	247
G102	779			20	14	4725	1.89	0.60	0.71	3311.97	303
G103	1030			25	4	3150	1.26	1.39	0.11	744.65	181
G104	1030	2500	50	25	6	3150	1.26	1.02	0.18	1263.22	204
G105	1030			25	8	3150	1.26	0.84	0.26	1860.35	226

G106	1030			25	10	3150	1.26	0.74	0.42	2992.96	290
G107	1030			25	12	3150	1.26	0.67	0.44	3132.93	253
G108	1030			25	14	3150	1.26	0.62	0.60	4199.16	291

Table 5 Full details of the current tapered BGCWs - Case II from Maupre Bridge

Girder	h_{wo} [mm]	h_{wi} [mm]	t_f [mm]	γ°	t_w [mm]	a [mm]	a/h_{wi}	λ_s	$\frac{M_{ul,FE}}{M_{pl}}$	$V_{ul,FE}$ [kN]	$\tau_{ul,FE}$ [MPa]
G109	1936	2500	50	10	4	3200	1.28	1.72	0.12	828.36	107
G110	1653				4	4800	1.92	1.72	0.15	670.83	101
G111	1371				4	6400	2.56	1.72	0.17	580.60	106
G112	1936				6	3200	1.28	1.18	0.23	1595.79	137
G113	1653				6	4800	1.92	1.18	0.30	1386.97	140
G114	1371				6	6400	2.56	1.18	0.33	1135.92	138
G115	1936				8	3200	1.28	0.91	0.35	2428.97	157
G116	1653				8	4800	1.92	0.91	0.46	2130.25	161
G117	1371				8	6400	2.56	0.91	0.50	1718.57	157
G118	1936				10	3200	1.28	0.76	0.45	3135.75	162
G119	1653				10	4800	1.92	0.76	0.63	2930.27	177
G120	1371				10	6400	2.56	0.76	0.69	2401.32	175
G121	1936				12	3200	1.28	0.65	0.59	4078.22	176
G122	1653				12	4800	1.92	0.65	0.82	3797.95	191
G123	1371				12	6400	2.56	0.65	0.89	3100.26	188
G124	1936				14	3200	1.28	0.58	0.74	5130.55	189
G125	1653				14	4800	1.92	0.58	0.96	4428.46	191
G126	1371				14	6400	2.56	0.58	1.01	3485.42	182
G127	1642			15	4	3200	1.28	1.79	0.10	685.07	104
G128	1213				4	4800	1.92	1.79	0.13	595.80	123
G129	784				4	6400	2.56	1.79	0.14	479.75	153
G130	1642				6	3200	1.28	1.23	0.19	1339.74	136
G131	1213				6	4800	1.92	1.23	0.24	1116.24	153
G132	784				6	6400	2.56	1.23	0.25	853.68	181
G133	1642				8	3200	1.28	0.95	0.30	2063.15	157
G134	1213				8	4800	1.92	0.95	0.36	1681.55	173
G135	784				8	6400	2.56	0.95	0.36	1258.33	201
G136	1642				10	3200	1.28	0.79	0.40	2741.39	167
G137	1213				10	4800	1.92	0.79	0.49	2270.28	187
G138	784				10	6400	2.56	0.79	0.36	1258.52	160
G139	1642				12	3200	1.28	0.68	0.53	3645.87	185
G140	1213				12	4800	1.92	0.68	0.62	2883.36	198

G141	784				12	6400	2.56	0.68	0.62	2154.46	229
G142	1642				14	3200	1.28	0.60	0.68	4697.59	204
G143	1213				14	4800	1.92	0.59	0.77	3565.36	210
G144	784				12	6400	2.56	0.68	0.95	3301.41	351
G145	1335				4	3200	1.28	1.85	0.13	897.58	168
G146	752				4	4800	1.92	1.85	0.11	514.56	171
G147	1335				6	3200	1.28	1.27	0.17	1210.07	151
G148	752				6	4800	1.92	1.27	0.20	927.11	205
G149	1335				8	3200	1.28	0.98	0.26	1805.55	169
G150	752				8	4800	1.92	0.98	0.29	1362.73	226
G151	1335			20	10	3200	1.28	0.81	0.36	2509.04	188
G152	752				10	4800	1.92	0.81	0.40	1826.27	243
G153	1335				12	3200	1.28	0.70	0.17	1210.07	76
G154	752				12	4800	1.92	0.70	0.49	2278.02	252
G155	1335				14	3200	1.28	0.62	0.57	3922.09	210
G156	752				14	4800	1.92	0.62	0.59	2717.07	258
G157	1007				4	3200	1.28	1.92	0.09	594.67	148
G158	1007				6	3200	1.28	1.32	0.15	1054.65	175
G159	1007			25	8	3200	1.28	1.02	0.23	1571.63	195
G160	1007				10	3200	1.28	0.84	0.31	2149.46	213
G161	1007				12	3200	1.28	0.73	0.39	2734.27	226
G162	1007				14	3200	1.28	0.65	0.49	3382.44	240

Table 6 Full details of the current tapered BGCWs - Case I from Dole Bridge

All of this tables, to present the results from 162 models. The first positive eigenmode which responds to the shear buckling mode was scaled to the above mentioned values in the nonlinear modelling, both Case I and Case II.

The first positive eigenmode is the first of all. In Case II, the first positive eigenmode, it should be seek even within 30 first modes. Almost all girders have interactive to exception girders with higher t_w. The buckling is not restricted in one panel, but goes across the fold line and extended to the neighbouring panel, as almost all of the results

3.5. Effect of aspect ratio of the web panels

Plate girders with flat web plates require the use of a series of transverse stiffeners in their fabrication. This is because the flat web panel buckles at a relatively low value of the applied shear force. Consequently, the webs are often reinforced with transversal stiffeners along their spans to increase their buckling strengths.

Accordingly, it is a well-known fact that the aspect ratio of the web panel (a/h_w) plays a key role in the shear strength of such girders (see for example Refs. [15-16]). On the other hand,

corrugated web plates have much higher buckling strengths compared with flat web plates because of their significant out-of-plane stiffness [2-6].

Hence, it is widely accepted that the aspect ratio of the web panels (a/h_w) has no effect on the ultimate shear stress ($\tau_{ul,FE}$) of prismatic BGCWs. This could easily be ensured by revising the available design shear strengths [3,6,8,12] where the a/h_w ratio does not exist.

On the other hand, this effect did not yet investigated in the tapered BGCWs. Therefore, the effect of the a/h_{w1} ratio on the shear behaviour of tapered BGCWs was investigated in this sub-section. However, tapered BGCWs with different a/h_{w1} ratios were generated herein by varying the span ratio (a) instead of dividing the shear span by using stiffeners to accord with bridge girders in reality.

In practice, the distance between vertical stiffeners is much greater than the web depth. Therefore, three ratios of a/h_{w1} greater than unity were considered; 1.28, 1.92 y 2.56 for Dole Bridge and 1.26, 1.89 y 2.52 for Maupre Bridge.

It can be seen from Table 4, 5 y 6 that increasing the ratio of a/h_{w1} of the girder leads to a considerable decrease in the ultimate shear strength ($V_{ul,FE}$).

The load against mid-span vertical deflection for selected girders is provided in Figure 15 as sample results from Dole Bridge. These girders (G109, G110 and G111) had an inclination angle of 10˚.

This figure shows that both the load and the initial shear stiffness considerably decrease as the aspect ratio increases.

It can additionally be observed that the failure is sudden and results from buckling for such BGCWs with relatively small web thickness. After the maximum load was achieved, considerable residual strength remains after failure.

a)

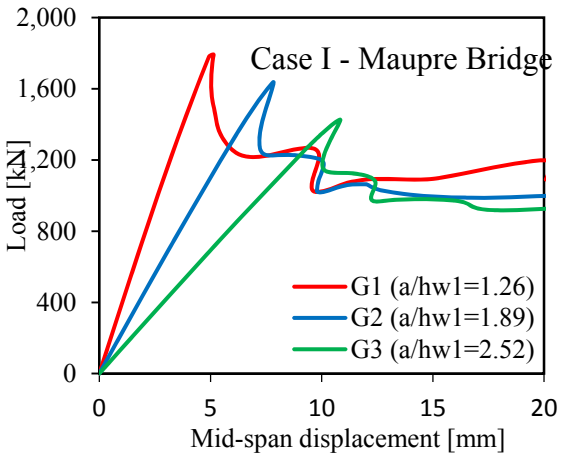

b)

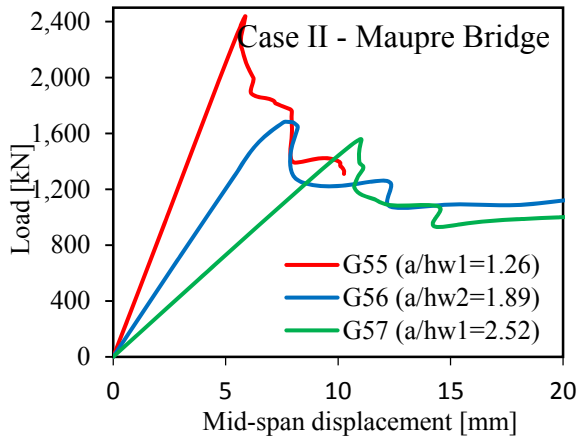

c)

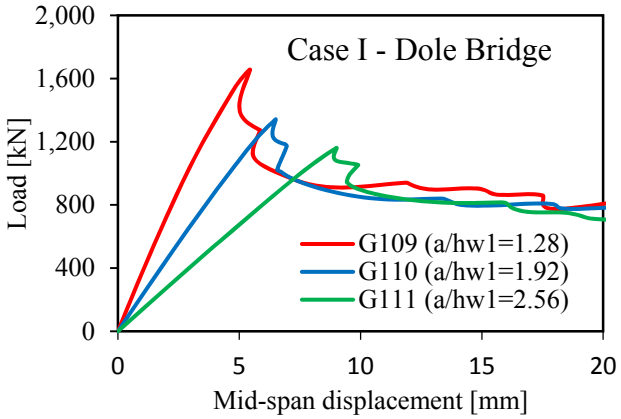

Figure 15 a) Load-mid-span deflection for girders G1, G2 and G3, belongs Case I-Maupre Bridge**, b)** Load-mid-span deflection for girders G55, G56 and G57, belongs Case II-Maupre Bridge, **c)** Load-mid-span deflection for girders G109, G110 and G111, and belongs Case I-Dole Bridge.

On the other hand, the variation of $\tau_{ul,FE}/\tau_y$ ratio with the aspect ratio for the tapered Maupre Bridge from Case I and Case II for flange slenderness ratio $b_f/2t_f = 5$ is given in Figure 16. As can be noticed, the $\tau_{ul,FE}/\tau_y$ ratios of the girders with the least inclination angle (i.e. $\gamma = 10°$) seem not to be affected by the change in the a/h_{wi} ratio similar to the case of prismatic girders.

For a value of $b_f/2t_f = 5$ ratio, this figure also demonstrates that tapered BGCWs with larger shear spans (i.e. girders with increased a/h_{wi} ratios) are more prone to shear deformations and, therefore, can relatively reach higher stresses with regard to their plastic shear resistances ($\tau_{ul,FE}/\tau_y$) compared to girders with less a/h_{wi} ratio specially for girders with large angle of inclination (i.e. $\gamma = 20°$). This is simply attributed to the very small web depth of the critical section of the girders (h_{wo}) compared to its length in the girders with smaller angles of inclinations; see Table 3, 4, y 5.

Figure 17 y 18 shows the stress distribution (of the middle surface of the webs) captured at the ultimate load of girders G1, G2, G3 from Case I and G55, G56, G57 from Case II, both belong to Maupre Bridge, as sample results.

Maupre Bridge – Case I

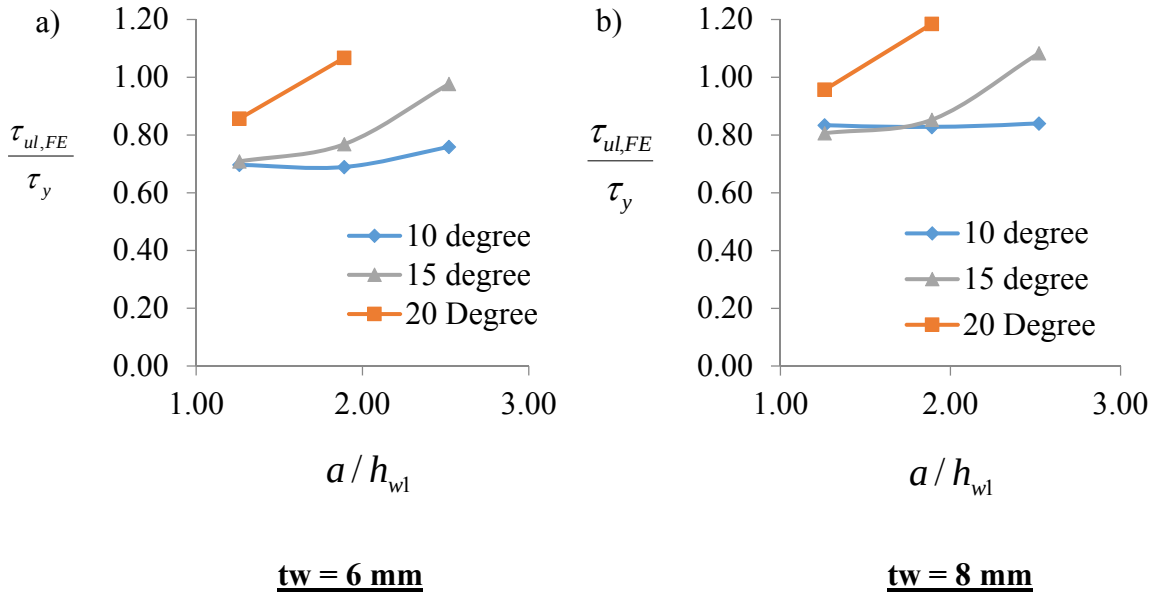

tw = 6 mm **tw = 8 mm**

Maupre Bridge – Case II

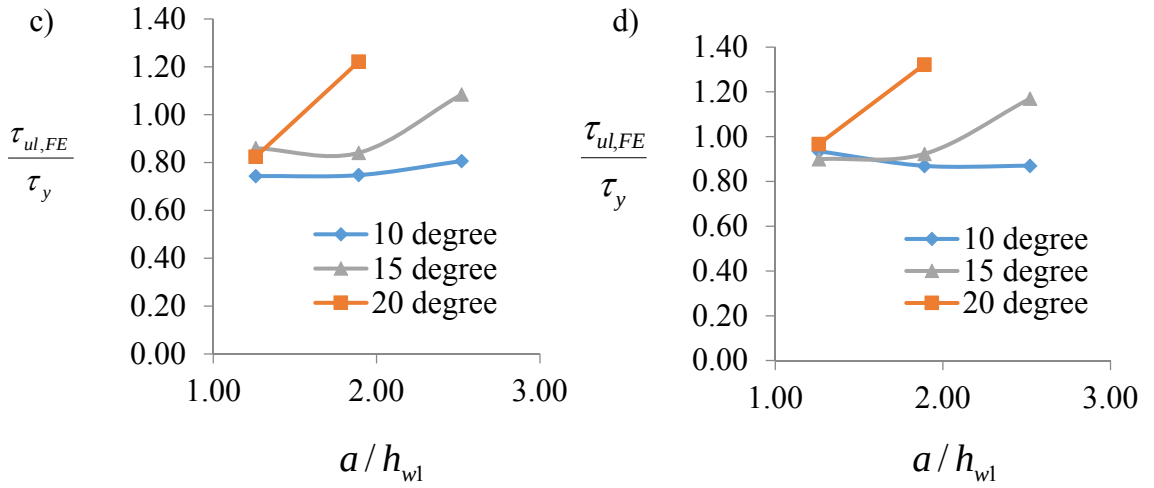

tw = 6 mm **tw = 8 mm**

Figure 16 Variation of $\tau_{ul,FE}/\tau_y$ with $Tan(\gamma)$ for tapered BGCWs for $b_f/2t_f = 5$ according to a) Case I from Maupre Bridge with tw = 6 mm, b) Case I from Maupre Bridge with tw = 8 mm, c) Case II from Maupre Bridge with tw = 6 mm, a) Case II from Maupre Bridge with tw = 8 mm

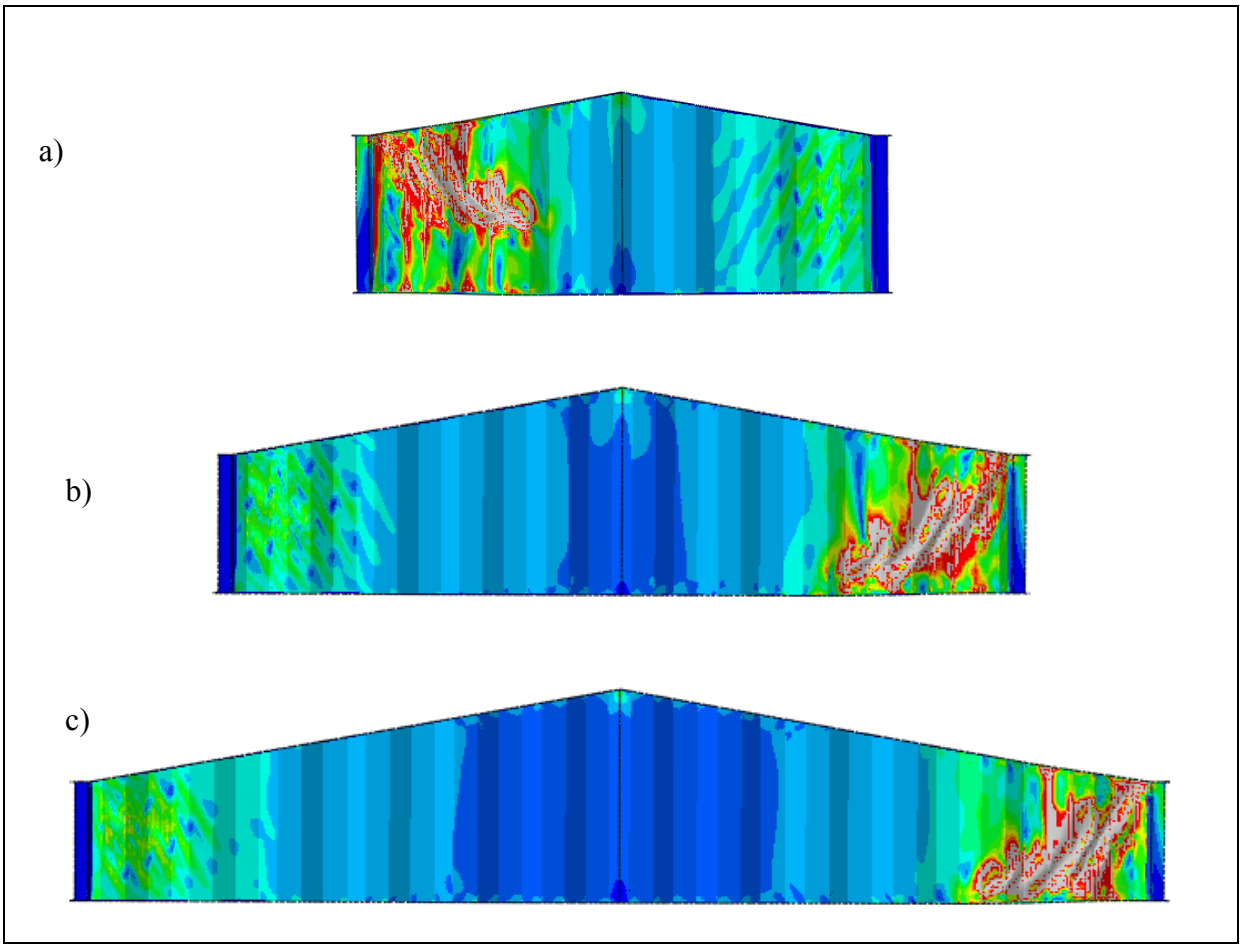

Figure 17 Stress contour of Girders a) G1, b) G2 and c) G3.

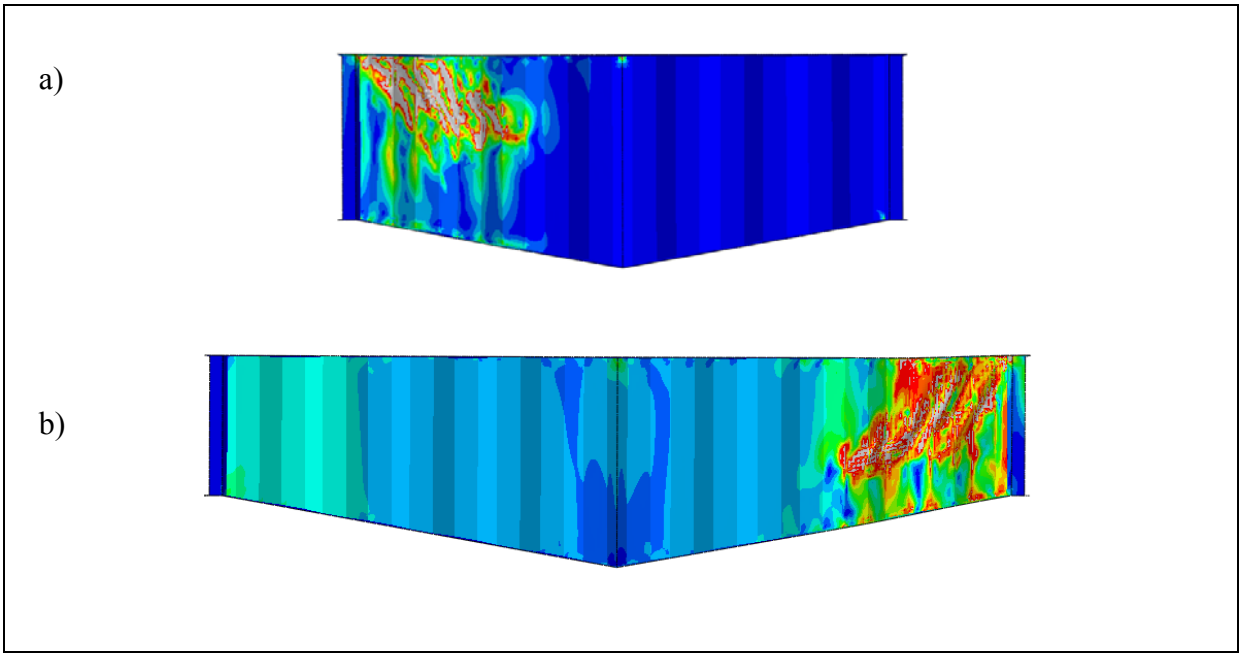

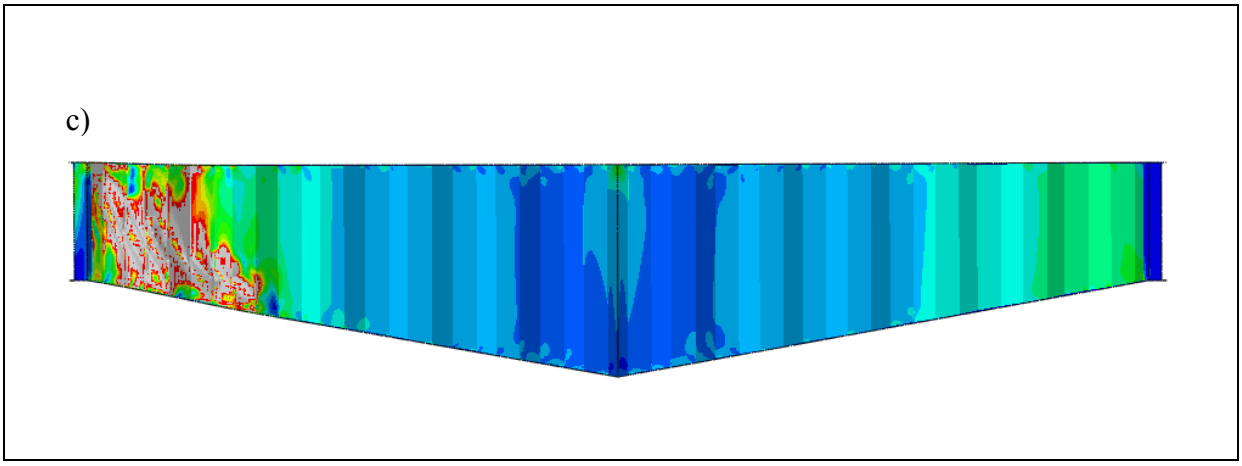

Figure 18 Stress contour of Girders a) G55, b) G56 and c) G57.

In the figure, regions with the gray contour represent the locations exceeding the yield strength of the material (355MPa), while the red, just surrounding the gray contour, shows the regions just yielded.

As can be seen, the plasticity spreads near the shorter edge of the shear panels as the shear stress is maximized. Also, it should be noted that the failure mode of the BGCWs does not show the propagation of shear plastic hinges (SPHs) at their top flange similar to those appear in plate girders with flat web plates [9].

It was recently understood [26,27] that the SPHs Figure 19 develop as a result of the differential shear deformation between the top and bottom flanges. It was taken from reference [25]. As the flat web plate buckles, the top flange undergoes downward displacement greater than that of the bottom.

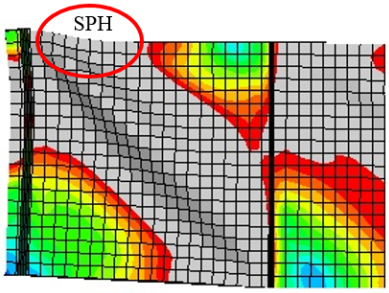

Figure 19 Developed shear plastic hinge in plate girders with flat webs [25]

This downward displacement, however, increases as the load increases leading to the development of diagonal tension field. Once the web has yielded, failure of the steel plate girder occurs when plastic hinges are formed in the flange due to the excessive downward displacement compared to that of the bottom.

This, however, not the case in BGCWs as they possess significant out-of-plane stiffness. Accordingly, the out-of-plane deformation of the corrugated webs is relatively limited. So, no relative shear deformation exits between both flanges to form the SPHs.

3.6. Effect of angle of the inclined flange

The influence of the inclined flange angle (γ) on the ultimate shear strength ($V_{ul,FE}$) and the load-mid-span deflection response of tapered BGCWs under shear loading was additionally studied. Three values of γ (10, 15, 20 and 25˚) were used confirming that the taper ratio (h_{wl}/h_{wo}) of the girders does not exceed 4 which was found to cover a large proportion of existing structures [19].

Herein, the maximum value of the taper ratio was 3.2 for the case of $\gamma = 25°$ and $a = 6300mm$ The applied load-mid-span vertical deflection relationships for sample results are provided in Figure 20.

This figure shows these relationships for girders G13, G31, G45 and G53 to Case I-Maupre Bridge and G67, G85, G99 and G107 to Case II-Maupre Bridge which have inclined flange angles of 10, 15, 20 and 25˚, respectively. It can be seen that increasing the inclined flange angle (γ) significantly reduces the ultimate shear strength of the tapered BGCWs, while the initial stiffness remains more or less the same.

a)

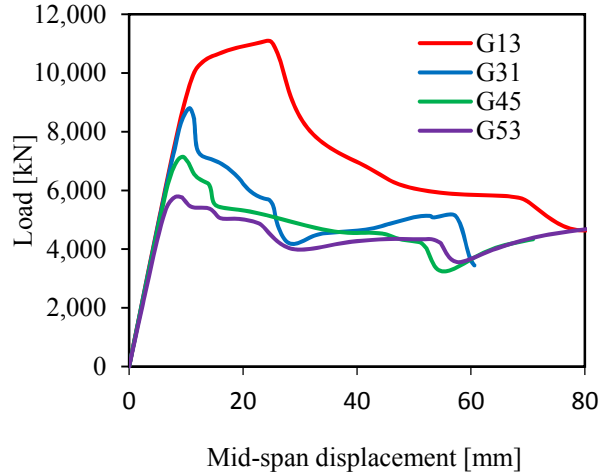

b)

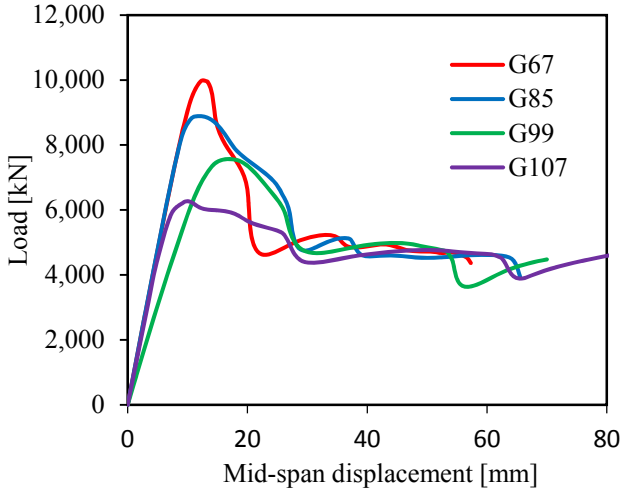

Figure 20 Load-mid-span deflection for girders a) G13, G31, G45 and G53 from Case I-Maupre Bridge and b) girders G67, G85, G99 and G107 from Case II-Maupre Bridge with tw=12 mm.

Additionally, it can be seen that all tapered BGCWs behave in a brittle manner irrespective of the value of γ with a considerable residual strength remaining after failure.

On the other hand, the influence of the flange angle of inclination on the normalized shear strength ($\tau_{ul,FE}/\tau_y$) of tapered BGCWs is shown in Figure 21 with flange slenderness ratio $b_f/2t_f = 5$.

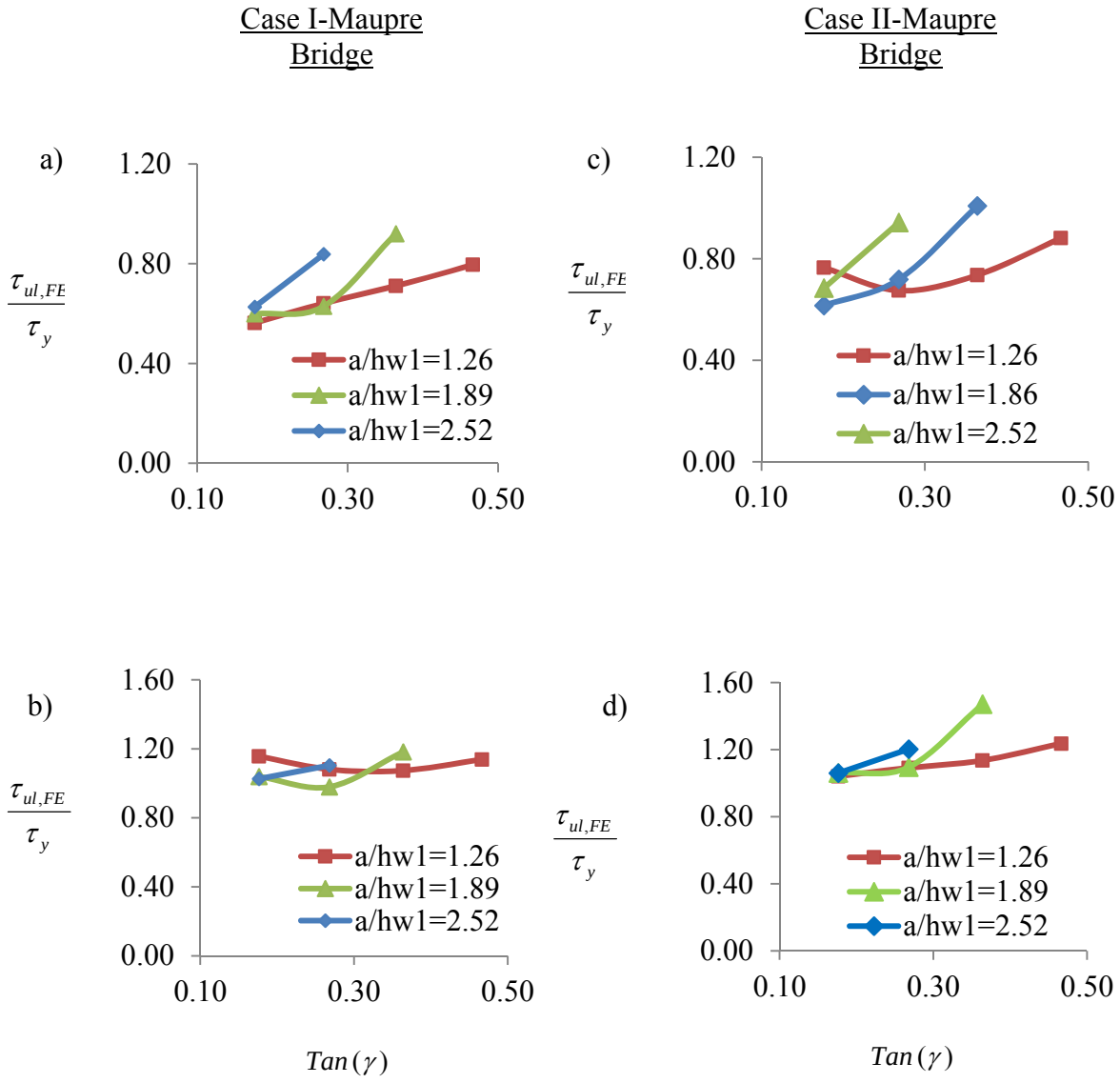

Figure 21 Variation of $\tau_{ul,FE}/\tau_y$ with $Tan(\gamma)$ for tapered BGCWs for. a) y b) from Case I-Maupre Bridge with tw = 4mm and tw =12 mm, respectively and c) y d) from Case I-Maupre Bridge with tw = 4mm and tw = 12 mm, respectively.

In this figure, the variation of the $\tau_{ul,FE}/\tau_y$ ratio is presented with respect to $Tan(\gamma)$. It is worth pointing out that tapered BGCWs with small values of γ (i.e. $\gamma = 10°$) have nearly the same $\tau_{ul,FE}/\tau_y$ ratios.

Also, Figure 21 shows an increase in the $\tau_{ul,FE}/\tau_y$ ratio for tapered BGCWs with the increase of γ. However, the rate of increase becomes higher for girders with increased aspect ratio (a/h_w). This increase results from the reduction in the critical web depth (h_{wo}) which becomes more pronounced in girders with larger a/h_w ratio.

The Figure 21 reveals that girders with thick flanges ($b_f/2t_f = 5$) experience a greater increase in the $\tau_{ul,FE}/\tau_y$ ratio. This observation may be attributed to the fact that thicker flanges provide more fixity at the juncture between the flanges and the webs leading to the increase of the shear strength of the girders. Figure 22 compares the stress distribution at the ultimate shear loads of the same selected girders presented previously in Fig. 21a (G13, G31, G45 and G53).

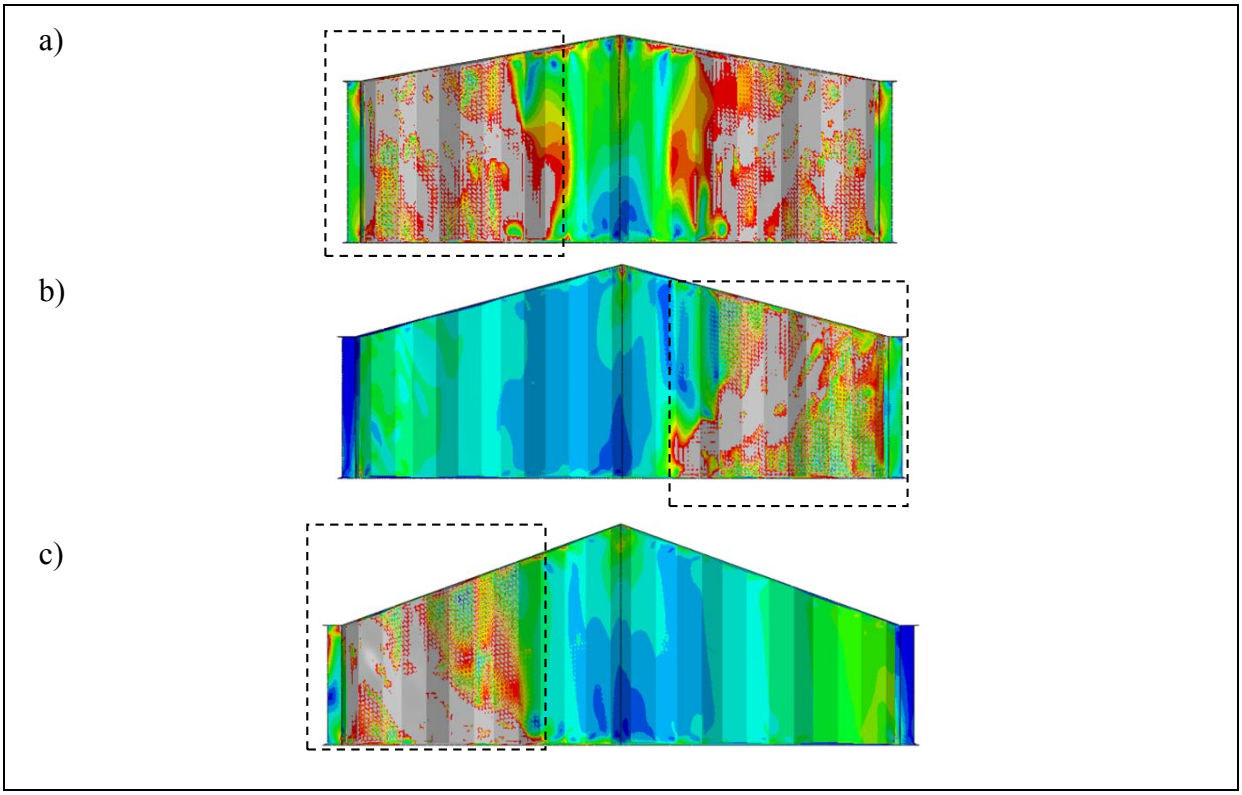

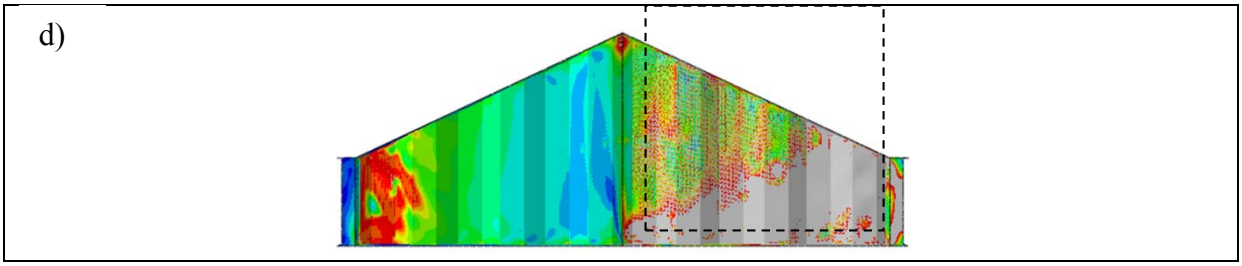

Figure 22 Stress contour of Girders a) G13, b) G31, c) G45 and d) G53 from Case I-Maupre Bridge.

Figure 23 compares the stress distribution at the ultimate shear loads of the same selected girders presented previously in Fig. 21b (G13, G31, G45 and G53).

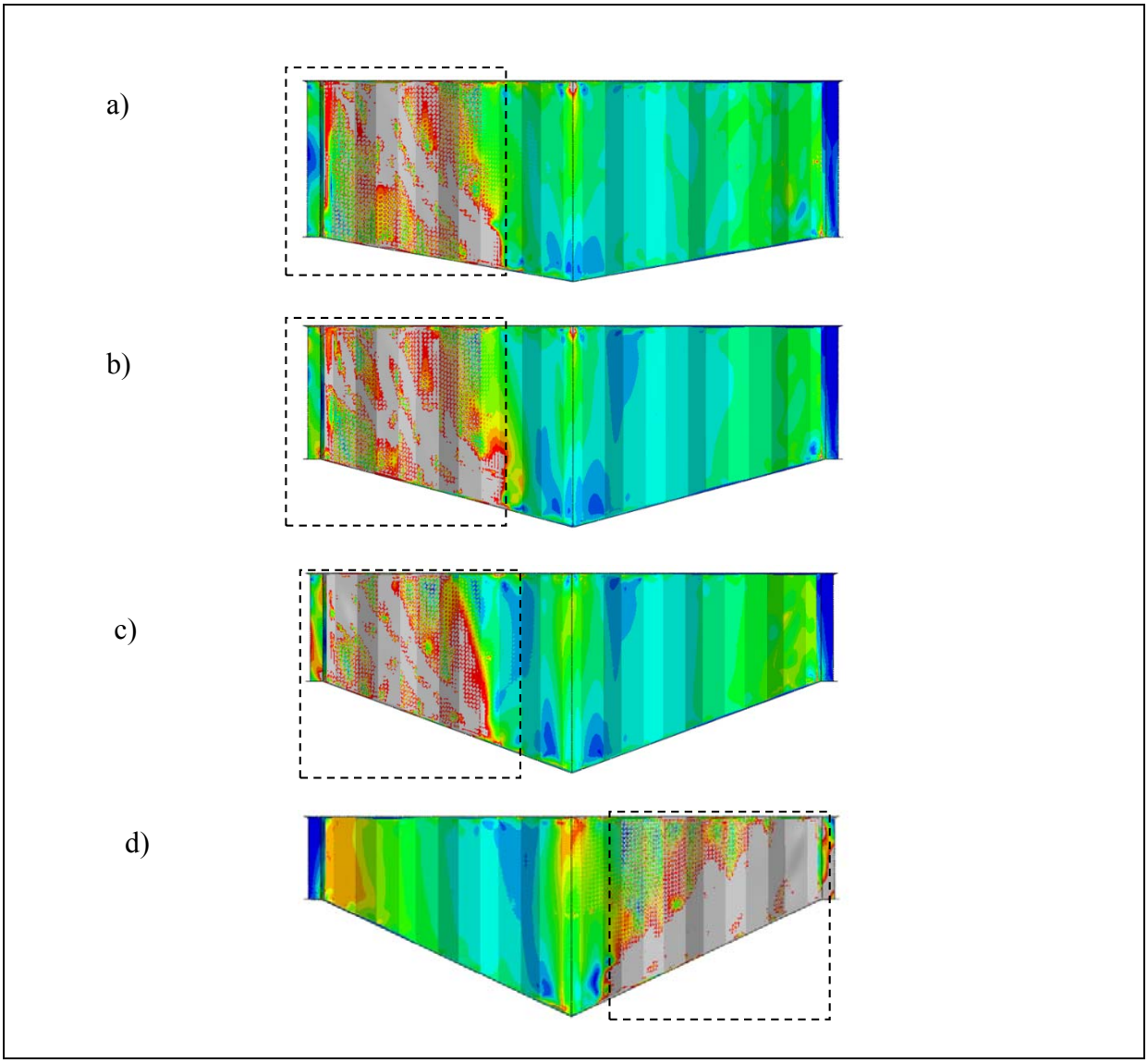

Figure 23 Stress contour of Girders a) G67, b) G85, c) G99 and d) G107 from Case II-Maupre Bridge.

As can be seen, the portions exceeding the yield strength of the material, enveloped by rectangles in the figure, extend in a wider range from the shear span by decreasing the angle of inclination. By decreasing the value of γ, the yielded portions become concentrated near the end supports where the shear stress is maximized.

Chapter 4. Design Proposal for Ultimate Shear Strength of Tapered Bridge Girders Corrugated Webs (BGCWs)

The interest to know which is the behaviour from BGCWs, and to compare with the proposal from literature, it is important since it allow checking the accuracy from equation 1, belongs to Moon et al [3], and whether it is necessary fit it.

To check this proposal, it need to vary the thickness web and the inclination angle of flange, in this way, to get new values from every case, and compare with the critical stress from nonlinear analysis $\tau_{ul,FE}$, On the other hand, the reliability of the design model for the full slenderness parameter range (greater than 0.6).

4.1. Case I from Maupre and Dole Bridge

In table 7 and 8, it can be seen the results of Case I from Maupre Bridge and Dole Bridge, respectively. The difference among bridges is shown in table 2, whereby, despite to study the same case, the results depend on shape profile, together with the change of thickness web, flange inclination angle and aspect ratio

Girder	λ_s	a/h_w	t_w [mm]	γ°	$\tau_{ul,FE}/\tau_y$	$\tau_{ul,\mathrm{Prop}}/\tau_y$	$\tau_{ul,FE}/\tau_{ul,\mathrm{Prop}}$
G1	1.25	1.26	4	10	0.56	0.60	0.94
G2	1.25	1.89	4	10	0.60	0.60	1.00
G3	1.25	2.52	4	10	0.63	0.60	1.05
G4	0.91	1.26	6	10	0.70	0.81	0.86
G5	0.91	1.89	6	10	0.69	0.81	0.85
G6	0.91	2.52	6	10	0.76	0.81	0.94
G7	0.75	1.26	8	10	0.83	0.91	0.92
G8	0.75	1.89	8	10	0.83	0.91	0.91
G9	0.75	2.52	8	10	0.84	0.91	0.93
G10	0.65	1.26	10	10	0.97	0.97	1.00
G11	0.65	1.89	10	10	0.89	0.97	0.92
G12	0.65	2.52	10	10	0.89	0.97	0.92
G13	0.59	1.26	12	10	1.16	1.01	1.15
G14	0.59	1.89	12	10	1.04	1.01	1.03
G15	0.59	2.52	12	10	1.03	1.01	1.02
G16	0.54	1.26	14	10	1.05	1.03	1.02
G17	0.54	1.89	14	10	1.06	1.03	1.03

G18	0.54	2.52	14	10	0.93	1.03	0.90
G19	1.30	1.26	4	15	0.64	0.57	1.13
G20	1.30	1.89	4	15	0.65	0.57	1.14
G21	1.30	2.52	4	15	0.84	0.57	1.47
G22	0.95	1.26	6	15	0.71	0.79	0.90
G23	0.95	1.89	6	15	0.77	0.79	0.98
G24	0.95	2.52	6	15	0.98	0.79	1.24
G25	0.78	1.26	8	15	0.81	0.89	0.91
G26	0.78	1.89	8	15	0.85	0.89	0.96
G27	0.78	2.52	8	15	1.08	0.89	1.22
G28	0.68	1.26	10	15	0.92	0.95	0.97
G29	0.68	1.89	10	15	0.95	0.95	1.00
G30	0.68	2.52	10	15	1.05	0.95	1.10
G31	0.61	1.26	12	15	1.08	0.99	1.09
G32	0.61	1.89	12	15	0.98	0.99	0.99
G33	0.61	2.52	12	15	1.10	0.99	1.11
G34	0.57	1.26	14	15	1.12	1.02	1.09
G35	0.57	1.89	14	15	1.00	1.02	0.98
G36	0.57	2.52	14	15	1.27	1.02	1.24
G37	1.35	1.26	4	20	0.71	0.54	1.32
G38	1.35	1.89	4	20	0.92	0.54	1.70
G39	0.98	1.26	6	20	0.86	0.76	1.12
G40	0.98	1.89	6	20	1.07	0.76	1.40
G41	0.81	1.26	8	20	0.96	0.87	1.10
G42	0.81	1.89	8	20	1.18	0.87	1.36
G43	0.70	1.26	10	20	1.00	0.94	1.07
G44	0.70	1.89	10	20	0.96	0.94	1.03
G45	0.64	1.26	12	20	1.07	0.98	1.10
G46	0.64	1.89	12	20	1.18	0.98	1.21
G47	0.59	1.26	14	20	1.08	1.01	1.07
G48	0.59	1.89	14	20	1.33	1.01	1.32
G49	1.40	1.26	4	25	0.80	0.51	1.56
G50	1.02	1.26	6	25	0.90	0.74	1.21
G51	0.84	1.26	8	25	0.98	0.85	1.14
G52	0.73	1.26	10	25	1.06	0.92	1.15
G53	0.66	1.26	12	25	1.14	0.96	1.18
G54	0.61	1.26	14	25	1.20	1.00	1.21

Table 7 Complete design curve - Case I from Maupre Bridge

Girder	λ_s	a/h_{wl}	t_w [mm]	γ°	$\tau_{ul,FE}/\tau_y$	$\tau_{ul,\mathrm{Prop}}/\tau_y$	$\tau_{ul,FE}/\tau_{ul,\mathrm{Prop}}$

G55	1.23	1.26	4	10	0.76	0.61	1.25
G56	1.23	1.89	4	10	0.62	0.61	1.00
G57	1.23	2.52	4	10	0.68	0.61	1.11
G58	0.90	1.26	6	10	0.74	0.82	0.91
G59	0.90	1.89	6	10	0.75	0.82	0.91
G60	0.90	2.52	6	10	0.81	0.82	0.99
G61	0.74	1.26	8	10	0.93	0.92	1.02
G62	0.74	1.89	8	10	0.87	0.92	0.95
G63	0.74	2.52	8	10	0.87	0.92	0.95
G64	0.64	1.26	10	10	1.01	0.97	1.04
G65	0.64	1.89	10	10	1.01	0.97	1.04
G66	0.64	2.52	10	10	0.95	0.97	0.98
G67	0.58	1.26	12	10	1.04	1.01	1.03
G68	0.58	1.89	12	10	1.06	1.01	1.05
G69	0.58	2.52	12	10	1.06	1.01	1.05
G70	0.53	1.26	14	10	1.08	1.04	1.04
G71	0.53	1.89	14	10	1.08	1.04	1.03
G72	0.53	2.52	14	10	0.95	1.04	0.91
G73	1.28	1.26	4	15	0.67	0.59	1.15
G74	1.28	1.89	4	15	0.72	0.59	1.23
G75	1.28	2.52	4	15	0.94	0.59	1.61
G76	0.93	1.26	6	15	0.86	0.80	1.08
G77	0.93	1.89	6	15	0.84	0.80	1.05
G78	0.93	2.52	6	15	1.08	0.80	1.36
G79	0.76	1.26	8	15	0.90	0.90	1.00
G80	0.76	1.89	8	15	0.92	0.90	1.03
G81	0.76	2.52	8	15	1.17	0.90	1.30
G82	0.67	1.26	10	15	1.03	0.96	1.07
G83	0.67	1.89	10	15	1.00	0.96	1.05
G84	0.67	2.52	10	15	1.37	0.96	1.43
G85	0.60	1.26	12	15	1.09	1.00	1.09
G86	0.60	1.89	12	15	1.10	1.00	1.10
G87	0.60	2.52	12	15	1.20	1.00	1.20
G88	0.55	1.26	14	15	1.10	1.03	1.07
G89	0.55	1.89	14	15	1.20	1.03	1.16
G90	0.55	2.52	14	15	1.38	1.03	1.34
G91	1.32	1.26	4	20	0.74	0.56	1.32
G92	1.32	1.89	4	20	1.01	0.56	1.81
G93	0.97	1.26	6	20	0.82	0.78	1.06
G94	0.97	1.89	6	20	1.22	0.78	1.58
G95	0.79	1.26	8	20	0.97	0.88	1.10

G96	0.79	1.89	8	20	1.32	0.88	1.50
G97	0.69	1.26	10	20	1.06	0.94	1.12
G98	0.69	1.89	10	20	1.40	0.94	1.49
G99	0.62	1.26	12	20	1.14	0.99	1.15
G100	0.62	1.89	12	20	1.47	0.99	1.49
G101	0.58	1.26	14	20	1.21	1.02	1.19
G102	0.58	1.89	14	20	1.48	1.02	1.46
G103	1.37	1.26	4	25	0.88	0.53	1.68
G104	1.00	1.26	6	25	1.00	0.75	1.32
G105	0.82	1.26	8	25	1.10	0.86	1.27
G106	0.72	1.26	10	25	1.42	0.93	1.53
G107	0.65	1.26	12	25	1.24	0.97	1.27
G108	0.60	1.26	14	25	1.42	1.00	1.42

Table 8 Complete design curve - Case I from Dole Bridge

The table 6 and 7, in some girders from Cases I can reach $\tau_{ul,FE}/\tau_y$ ratios greater than unity. This means that their materials can effectively be utilized.

In the figure 21a and 21b, it can be seen the results of Case I from Maupre Bridge and Dole Bridge, respectively.it shows the relationship between the $\tau_{ul,FE}/\tau_y$ ratio against the parameter λ_s. The dashed line represents the design strength given by Equation. 1.

a)

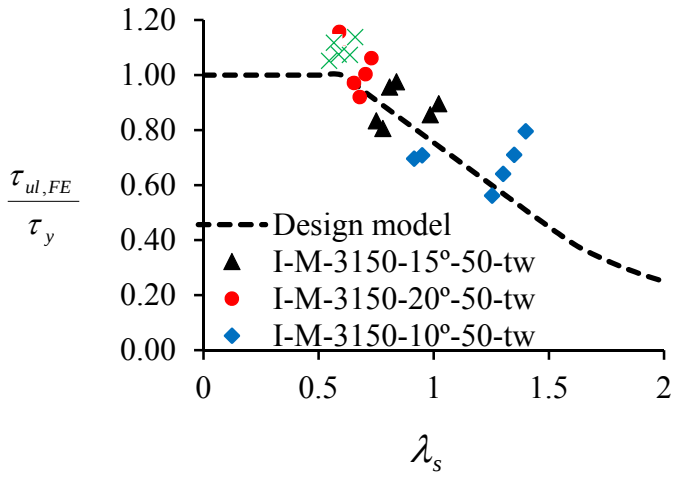

b)

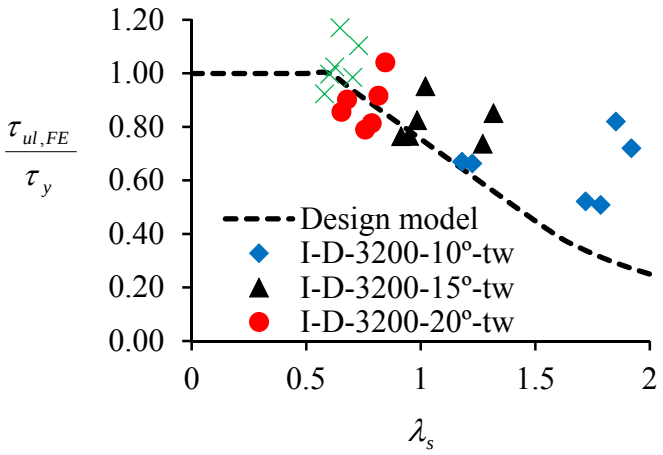

Figure 24 Design model versus slenderness parameter a) Case I from Maupre Bridge, and b) Case I from Dole Bridge.

It is worth pointing that the range of λ_s vary from 0.54 to 1.4 to Maupre Bridge and from 0.58 to 1.92 to Dole Bridge. The high value of shear buckling parameter of the corrugated webs belongs to girders with lower thickness value, represent the third stage $\sqrt{2} < \lambda_s$, from equation 1[3].

Most of results are conservative, it can be noticed that they are placed over the design model curve, nevertheless, it has some of them under the curve, for both Maupre Bridge as Dole Bridge, it mean that it possible fitting the design model curve to Case I.

4.2. Case II from Maupre Bridge

In table 9, it can be seen the results of Case II from Maupre Bridge. Here, the results depend on just Maupre Bridge shape profile, together with the change of thickness web, flange inclination angle and aspect ratio. It worth pointing that the results from this table are new for literature.

Girder	λ_s	a/h_{wl}	t_w [mm]	γ°	$\tau_{ul,FE}/\tau_y$	$\tau_{ul,Prop}/\tau_y$	$\tau_{ul,FE}/\tau_{ul,Prop}$
G109	1.72	1.28	4	10	0.52	0.76	0.68
G110	1.72	1.92	4	10	0.49	0.76	0.65
G111	1.72	2.56	4	10	0.52	0.76	0.68
G112	1.18	1.28	6	10	0.67	0.64	1.04
G113	1.18	1.92	6	10	0.68	0.64	1.06
G114	1.18	2.56	6	10	0.67	0.64	1.05
G115	0.91	1.28	8	10	0.77	0.81	0.95
G116	0.91	1.92	8	10	0.79	0.81	0.97
G117	0.91	2.56	8	10	0.76	0.81	0.95
G118	0.76	1.28	10	10	0.79	0.90	0.87
G119	0.76	1.92	10	10	0.86	0.90	0.96
G120	0.76	2.56	10	10	0.85	0.90	0.95

G121	0.65	1.28	12	10	0.86	0.97	0.89
G122	0.65	1.92	12	10	0.93	0.97	0.97
G123	0.65	2.56	12	10	0.92	0.97	0.95
G124	0.58	1.28	14	10	0.92	1.00	0.92
G125	0.58	1.92	14	10	0.93	1.00	0.93
G126	0.58	2.56	14	10	0.89	1.00	0.89
G127	1.79	1.28	4	15	0.51	0.75	0.68
G128	1.79	1.92	4	15	0.60	0.75	0.80
G129	1.79	2.56	4	15	0.75	0.75	1.00
G130	1.23	1.28	6	15	0.66	0.62	1.08
G131	1.23	1.92	6	15	0.75	0.62	1.21
G132	1.23	2.56	6	15	0.88	0.62	1.44
G133	0.95	1.28	8	15	0.77	0.79	0.98
G134	0.95	1.92	8	15	0.85	0.79	1.08
G135	0.95	2.56	8	15	0.98	0.79	1.24
G136	0.79	1.28	10	15	0.81	0.89	0.92
G137	0.79	1.92	10	15	0.91	0.89	1.03
G138	0.79	2.56	10	15	0.78	0.89	0.88
G139	0.68	1.28	12	15	0.90	0.95	0.95
G140	0.68	1.92	12	15	0.97	0.95	1.01
G141	0.68	2.56	12	15	1.12	0.95	1.17
G142	0.60	1.28	14	15	1.00	1.00	1.00
G143	0.59	1.92	14	15	1.02	1.00	1.02
G144	0.68	2.56	12	15	1.71	0.95	1.80
G145	1.85	1.28	4	20	0.82	0.73	1.12
G146	1.85	1.92	4	20	0.83	0.73	1.14
G147	1.27	1.28	6	20	0.74	0.59	1.25
G148	1.27	1.92	6	20	1.00	0.59	1.70
G149	0.98	1.28	8	20	0.82	0.76	1.08
G150	0.98	1.92	8	20	1.10	0.76	1.45
G151	0.81	1.28	10	20	0.92	0.87	1.06
G152	0.81	1.92	10	20	1.18	0.87	1.36
G153	0.70	1.28	12	20	0.98	0.94	1.05
G154	0.70	1.92	12	20	1.23	0.94	1.31
G155	0.62	1.28	14	20	1.02	0.98	1.04
G156	0.62	1.92	14	20	1.26	0.98	1.28
G157	1.92	1.28	4	25	0.72	0.72	1.00
G158	1.32	1.28	6	25	0.85	0.56	1.52
G159	1.02	1.28	8	25	0.95	0.74	1.28
G160	0.84	1.28	10	25	1.04	0.85	1.23
G161	0.73	1.28	12	25	1.10	0.92	1.20

G162	0.65	1.28	14	25	1.17	0.97	1.21

Table 9 Complete design curve - Case II from Maupre Bridge

In general terms, the values regarding table 7, 8 y 9 presents the ultimate stresses of the generated models compared with that of the proposed equation ($\tau_{ul,FE} / \tau_{ul,Prop}$).

In the figure 25, it can be seen the results of Case II from Maupre Bridge, it shows the relationship between the $\tau_{ul,FE}/\tau_y$ ratio against the parameter λ_s. The dashed line represents the design strength given by Equation. 1.

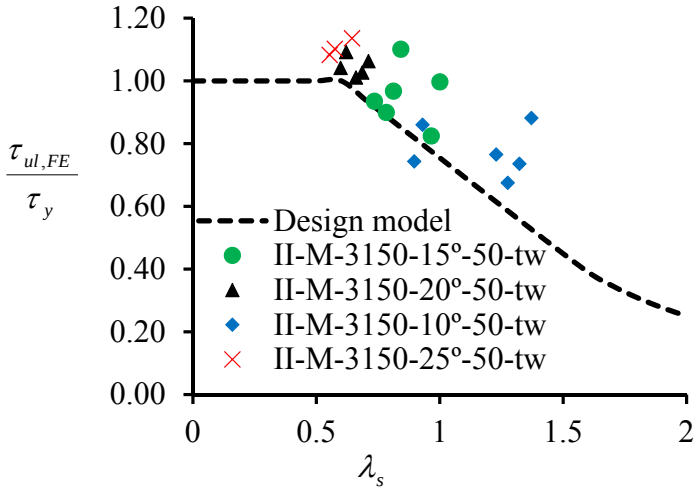

Figure 25 Design model versus slenderness parameter - Case II from Maupre Bridge.

The values in their majority are close to the unit or greater than this one, which it means that the values proposed equation 1 are conservative. It is further, the prediction is conservative, even when it increase the angle of inclination of flange or increase the thickness web, and however it provides a lower bound for the shear strength of tapered BGCWs.

Chapter 5. Fitted Design Proposal Curve for Ultimate Shear Strength of Tapered Bridge Girders Corrugated Webs (BGCWs)

From real profiles, both as Maupre as Dole, trying to know certain points within the results before obtained, by varying the dimensions of the real profile with not real dimensions which may help us understanding how affects the shape of the wave in the shear force resistant.

In table 10, it present the dimension from 16 girders analysed, it can be noticed that the angle among panels from profile shape vary from 7º to 90º, this allows taking in account a great range of possibilities, in this way, to set up the new design curve model, whether it is necessary.

BGCWs	b [mm]	d [mm]	c [mm]	q [mm]	s [mm]	hr [mm]	α°
G163	525.0	0.00	150.0	1050.0	1350.0	150.0	90.0
G164	404.5	120.5	192.4	1050.0	1193.8	150.0	51.2
G165	284.0	241.0	256.7	1050.0	1081.4	90.0	20.5
G166	284.0	241.0	242.9	1050.0	1053.7	30.0	7.1
G167	525.0	0.00	150.0	1050.0	1350.0	150.0	90.0
G168	404.5	120.5	192.4	1050.0	1193.8	150.0	51.2
G169	284.0	241.0	256.7	1050.0	1081.4	90.0	20.5
G170	284.0	241.0	242.9	1050.0	1053.7	30.0	7.1
G171	800.0	0.00	220.0	1600.0	2040.0	220.0	90.0
G172	615.0	185.0	287.9	1600.0	1805.8	220.0	50.0
G173	430.0	370.0	402.0	1600.0	1664.0	157.0	23.0
G174	430.0	370.0	375.3	1600.0	1610.6	63.0	9.7
G175	800.0	0.00	220.0	1600.0	2040.0	220.0	90.0
G176	615.0	185.0	287.9	1600.0	1805.8	220.0	50.0
G177	430.0	370.0	402.0	1600.0	1664.0	157.0	23.0
G178	430.0	370.0	375.3	1600.0	1610.6	63.0	9.7

Table 10 Dimensions from different profile shapes.

In figure 26 and 27, it can be seen graphically the profile shapes of interest to this study. It trying to get the behaviour near to flat panels, and to notice from buckling mode and nonlinear behaviour.

In figure 26 ,The analyse considers solely 15º as inclination angle of flange and 1.26 or 1.28 depending on profile shape base, Maupre according to Case I.

The results of $\tau_{ul,FE}$ are presented in table 11, this results are added to the results before obtained, in this way, to have a complete overview and to be able to predict the behaviour of a wide range of beams

Also, in the figure 26, it can be seen the results of Case I from different non real profile shapes, it shows the relationship between the $\tau_{ul,FE}/\tau_y$ ratio against the parameter λ_s. The dashed line represents the design strength given by Equation. 1.

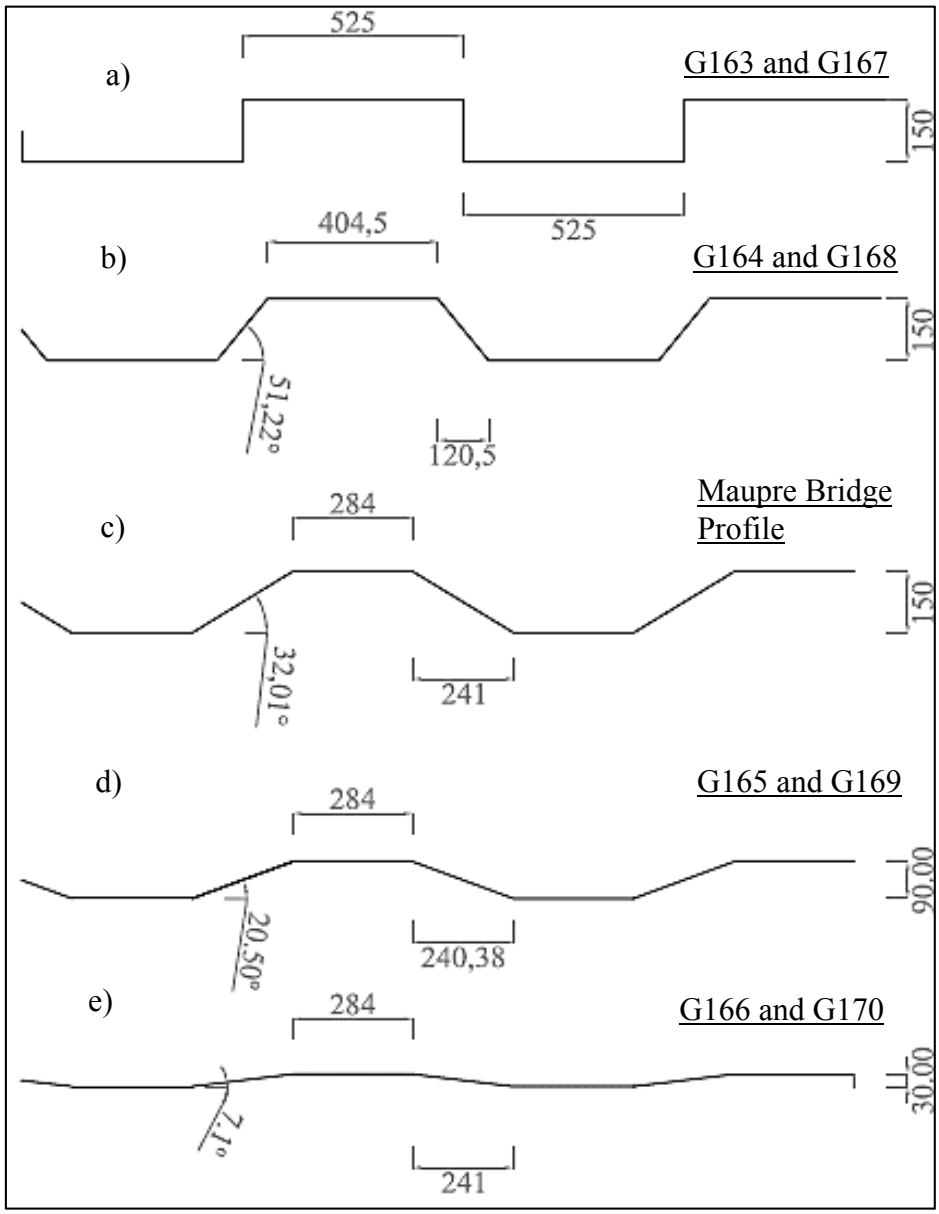

Figure 26 Different profile based in Maupre Bridge Profile.

In figure 27, the analyse considers solely 15º as inclination angle of flange and 1.26 or 1.28 depending on profile shape base, Doles regarding to Case I.

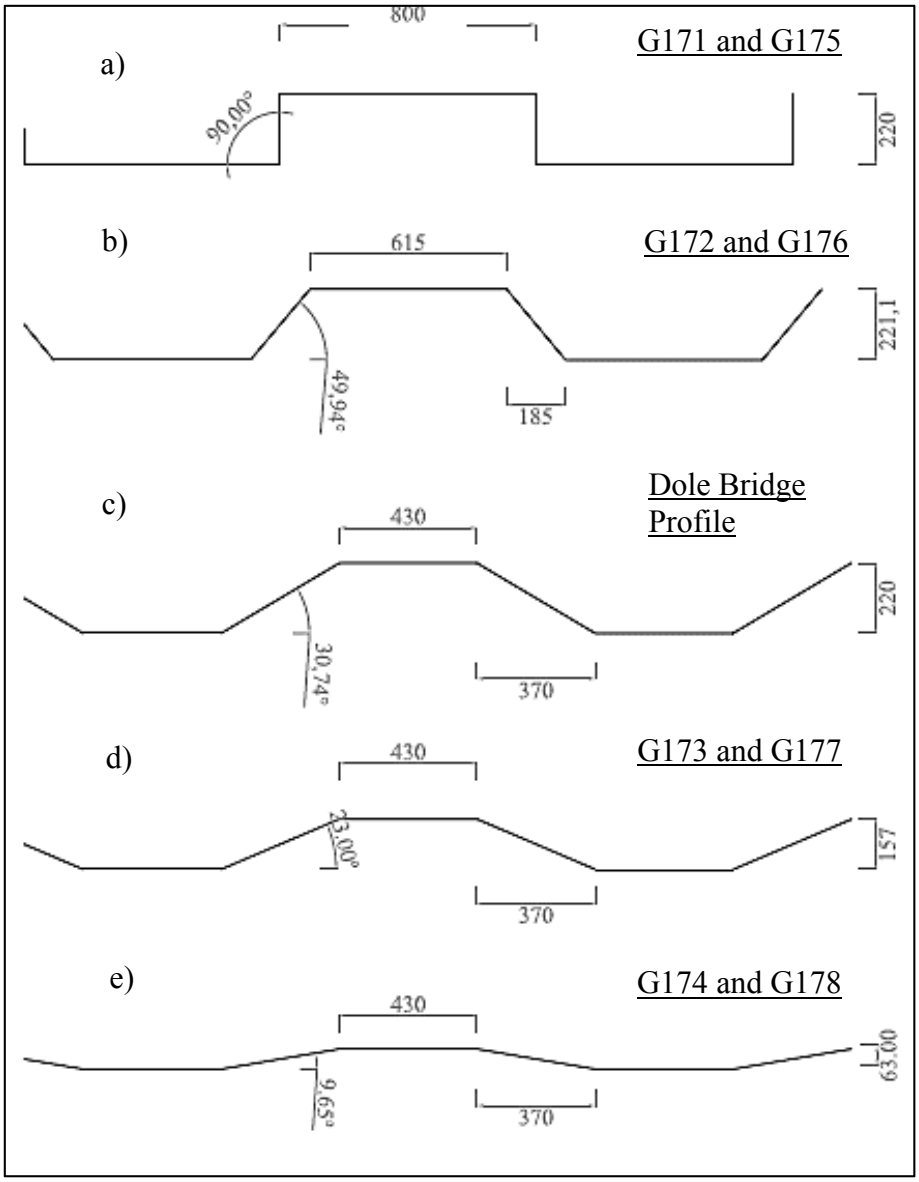

Figure 27 Different profile based in Dole Bridge Profile.

Girder	h_{wo} [mm]	h_{wi} [mm]	t_f [mm]	$\gamma°$	t_w [mm]	a [mm]	a/h_{wi}	λ_s	$\frac{M_{ul,FE}}{M_{pl}}$	$V_{ul,FE}$ [kN]	$\tau_{ul,FE}$ [MPa]
G163	1656	2500	50	15	6	3150	1.26	1.49	0.24	1664	168
G164	1656	2500	50	15	6	3150	1.26	1.20	0.23	1645	166
G165	1656	2500	50	15	6	3150	1.26	1.13	0.20	1435	144
G166	1656	2500	50	15	6	3150	1.26	2.07	0.23	1596	161
G167	1656	2500	50	15	12	3150	1.26	0.82	0.30	2103	106
G168	1656	2500	50	15	12	3150	1.26	0.70	0.60	4242	214
G169	1656	2500	50	15	12	3150	1.26	0.80	0.54	3810	192

G170	1656	2500	50	15	12	3150	1.26	1.66	0.48	3385	170
G171	1642	2500	50	15	6	3200	1.28	2.17	0.21	1423	144
G172	1642	2500	50	15	6	3200	1.28	1.69	0.20	1408	143
G173	1642	2500	50	15	6	3200	1.28	1.27	0.20	1412	143
G174	1642	2500	50	15	6	3200	1.28	1.59	0.12	824	84
G175	1642	2500	50	15	12	3200	1.28	1.11	0.39	2712	138
G176	1642	2500	50	15	12	3200	1.28	0.89	0.34	2371	120
G177	1642	2500	50	15	12	3200	1.28	0.74	0.52	3587	182
G178	1642	2500	50	15	12	3200	1.28	1.09	0.53	3681	187

Table 11 Results of $\tau_{ul,FE}$ from different profile shapes.

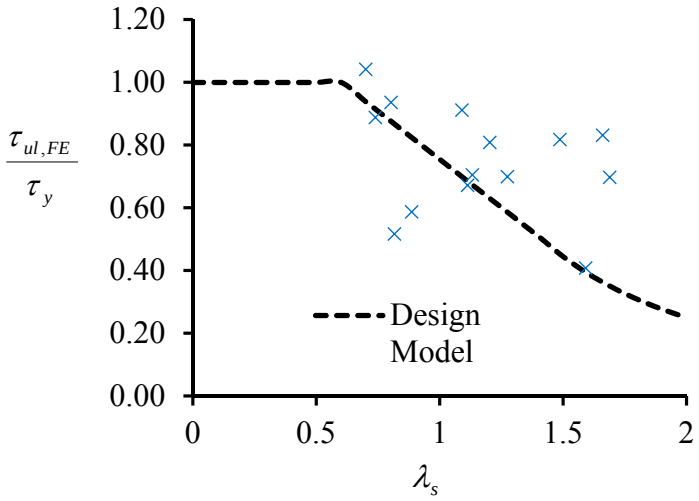

Figure 28 Design model versus slenderness parameter - Case I from Different Profile

It is possible to notice that as the angle between panels decrease, the ultimate shear decreases due to the fact that the web has much more rigidity. It is worth pointing that the web with lower angle among panels has the behaviour as flat panel, as can be seen in figure 26 and 27.

The distribution of S11 in girder G174 is quite different from that of girder G177. Figure 26A shows that, along the diagonal line of each fold, the stress concentration of S11 is very high, as can be clearly noticed.

Figure 30a shows the distribution of axial stress S11 in girder G177. It can be noticed that the flanges take nearly all the axial stress and the web has nearly zero axial stress, which is clearly shown in it. The axial stress in the web is close to that of the flange only in a very small area close to the welding line where web is connected to the flange, as at this point, webs tend to be stressed in the similar way as the flange because of the constraint due to welding.

The shear stress S12 in girder G174 is distributed evenly along the whole web panel, except a very small region of stress concentration at inclined fold as can be seen in Figure 29b. The reason for the higher shear stress in this region is that this fold has the maximum width, but the

shear stress S12 in G177 is not evenly distributed in the web, it should be because the profile shape is far away from flat panel.

The shear stress along the side of the flange is nearly zero, as can be notice in figure 29b y 30b; it is clearly that almost all the shear force is taken by the web.

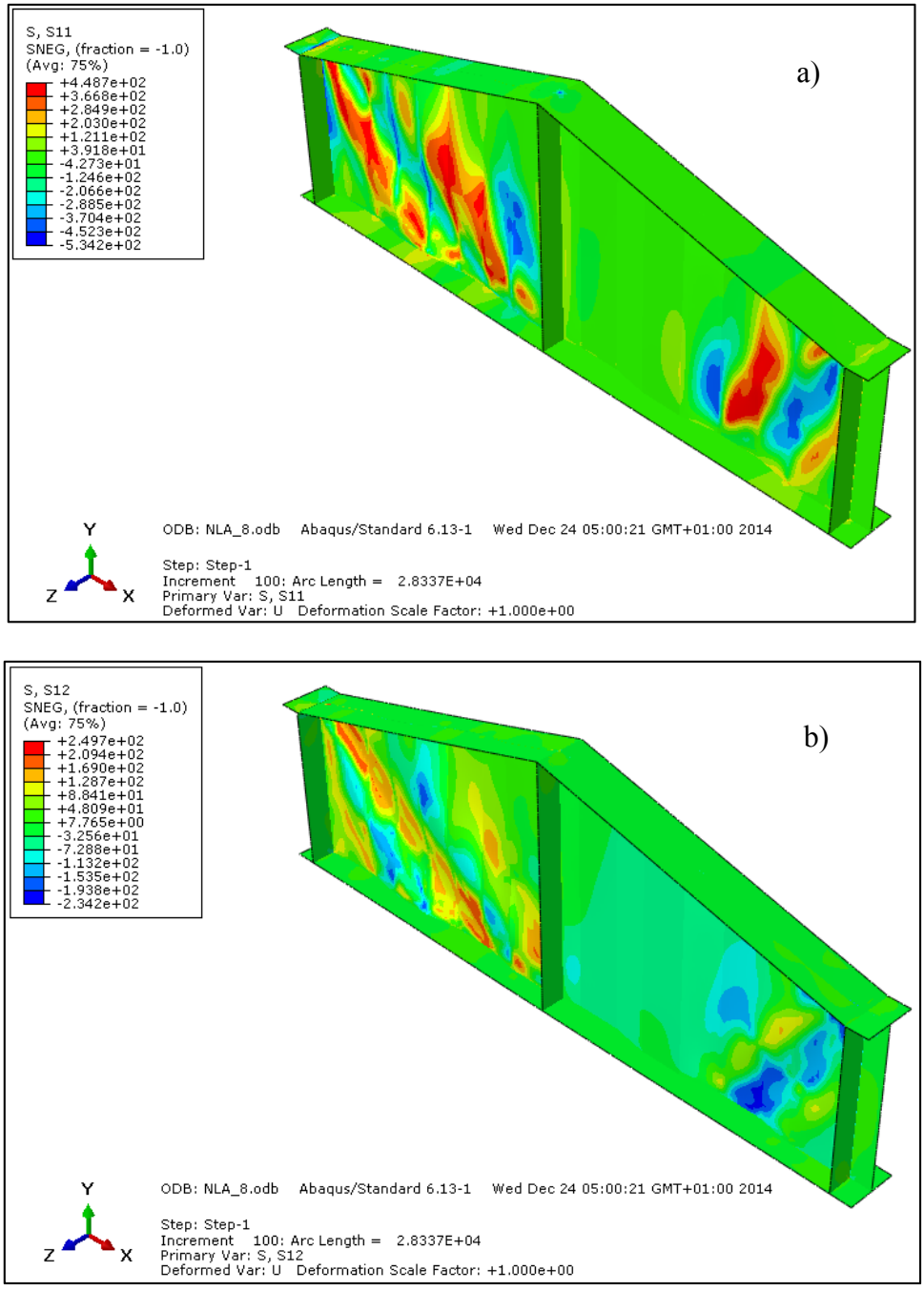

Figure 29 Stress contour a) S11 and b) S22 from G174.

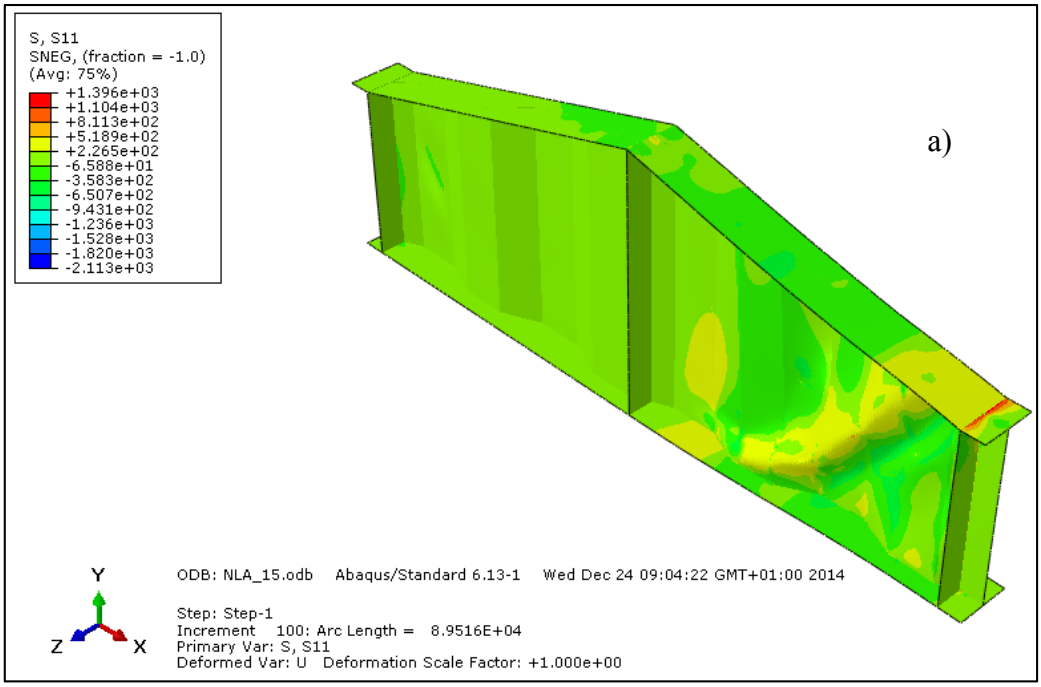

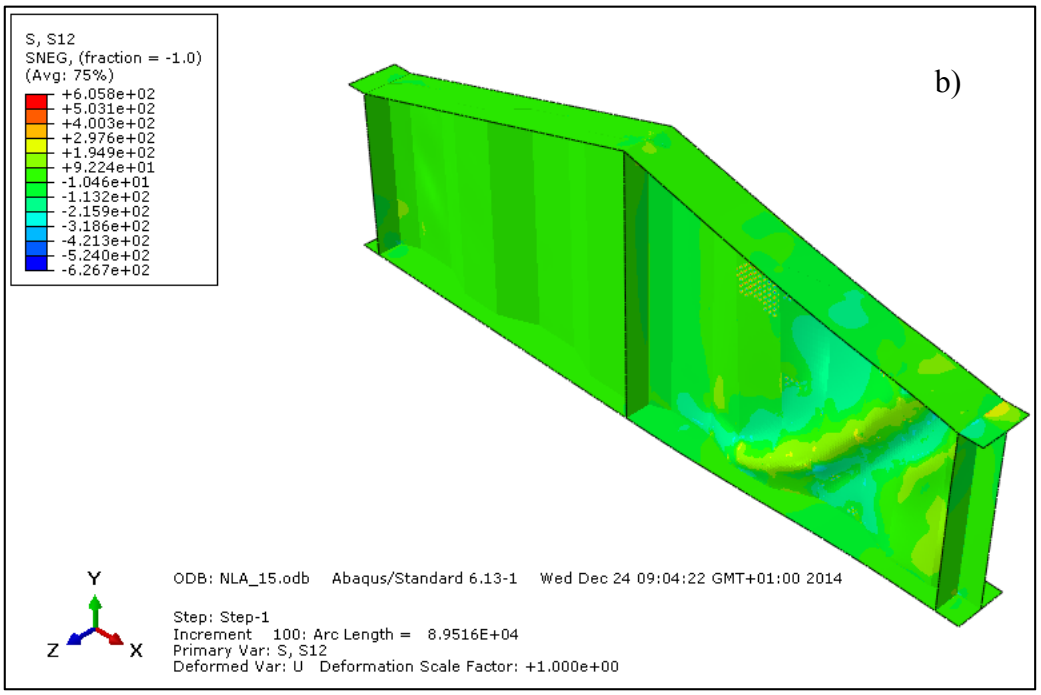

Figure 30 Stress contour a) S11 and b) S22 from G177.

5.1. Fitted Design Model Curve

Now, it graphics are all the points on the curve of the design model, found by adding up the points for different profiles. Figure 31 presents Design model versus slenderness parameter, considering all girders.

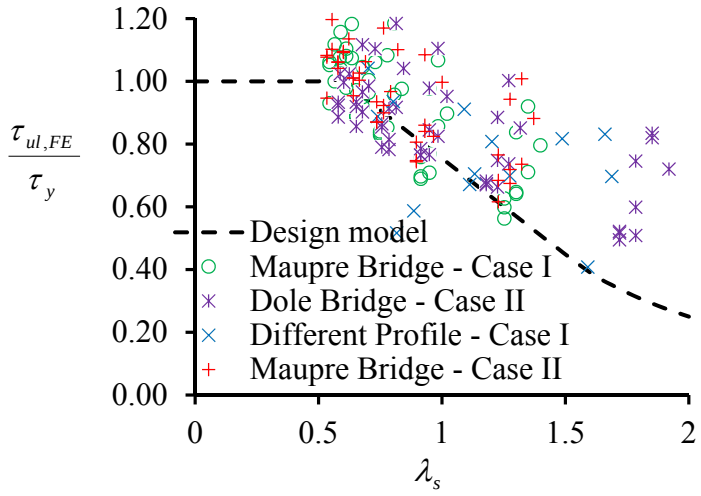

Figure 31 Design model versus slenderness parameter – All Data

Worldwide, many tests have been conducted on corrugated web girders and both local and global shear buckling modes have been observed, depending on the web geometry.

Shear capacity equations have been proposed based on classical elastic shear buckling theory and shear yielding, with inelastic transition regions. But the available data are most often based on tests of small beams with material thickness is generally well below what would be expected in practice, as it can be seen in table 1.

Now, it focus in the uncertainty region, inelastic transition region, second stage from equation 1. In table 12, it is provided the average (Ave), and coefficient of variation (COV) from the results belong to a) $\lambda_s \leq 0.6$, b) $0.6 < \lambda_s \leq \sqrt{2}$ and c) $\sqrt{2} < \lambda_s$.

a)

	$\tau_{ul,FE}/\tau_y$	$\tau_{ul,\text{Prop}}/\tau_y$	$\tau_{ul,FE}/\tau_{ul,\text{Prop}}$
Ave	1.11	1.02	1.09
COV	0.19	0.02	0.18

b)

	$\tau_{ul,FE}/\tau_y$	$\tau_{ul,\text{Prop}}/\tau_y$	$\tau_{ul,FE}/\tau_{ul,\text{Prop}}$
Ave	0.93	0.83	1.14
COV	0.20	0.14	0.22

c)

	$\tau_{ul,FE}/\tau_y$	$\tau_{ul,\text{Prop}}/\tau_y$	$\tau_{ul,FE}/\tau_{ul,\text{Prop}}$
Ave	0.67	0.75	0.89
COV	0.15	0.04	0.21

Table 12 Statistics values from a) $\lambda_s \leq 0.6$, b) $0.6 < \lambda_s \leq \sqrt{2}$ and c) $\sqrt{2} < \lambda_s$

Generally, the first region is accurately presented, the second region is not, with big variations ranging from conservative to non-conservative results. In the third one, the proposed equation is too much conservative. According, it will need to modify the equation by raising the curve upwards.

Regarding to the cloud of points, it is proposed to fit the curve of equation 1, with the equation 28 as follows:

$$\frac{\tau_{ul,Prop}}{\tau_y} = C_T \begin{cases} 1.0 & : \lambda_s \le 0.6 \\ 1 - 0.407(\lambda_s - 0.8) & : 0.6 < \lambda_s \le \sqrt{2} \\ 1.25\dfrac{1}{\lambda_s^2} & : \sqrt{2} < \lambda_s \end{cases} \tag{28}$$

In figure 32, it can be seen that the fitted curve involves all the points and it places them on the side of safety, both case I and case II from Maupre and Dole Bridge.

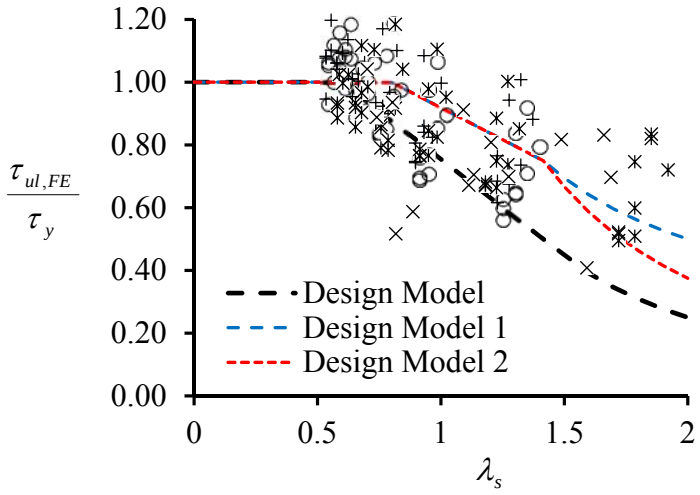

Figure 32 Fitted design model.

5.2. Illustrative Example

An example is presented in this section to explain the application of the design procedure proposed for tapered BGCWs. The example used the modelled tapered BGCW which has Maupre Bridge web corrugation dimensions; see Table 2. The web is 8 mm thickness. The tapered BGCW is of Case II and its inclination angle is 15º. Young's modulus and Poisson's ratio are 210 GPa and 0.3, respectively. To calculate the value of $\tau_{ul,Prop}$, the following procedures should be made:

The elastic local shear buckling stress of the prismatic corrugated web ($\tau_{cr,L}$) is to be calculated as:

$$\tau_{cr,L} = k_L \frac{\pi^2 E}{12(1-\nu^2)}\left(\frac{t_w}{w}\right)^2 = 5.34 \times \frac{\pi^2 \times 210000}{12(1-0.3^2)}\left(\frac{8}{284}\right)^2 = 805\,MPa$$

To calculate the elastic global shear buckling stress of the prismatic corrugated web ($\tau_{cr,G}$) the following should be made:

$$q = 2b + 2d = 2 \times 284 + 2 \times 241 = 1050$$

$$s = 2b + 2c = 2 \times 284 + 2 \times 284 = 1136$$

$$D_x = \frac{q}{s}\cdot\frac{Et_w^3}{12} = \frac{1050}{1136} \times \frac{210000 \times 8^3}{12} = 8{,}281{,}690{.}14\ \text{N mm}$$

$$I_y = 2bt_w\left(\frac{h_r}{2}\right)^2 + \frac{t_w h_r^3}{6\sin\alpha} = 2 \times 284 \times 8 \times \left(\frac{150}{2}\right)^2 + \frac{8 \times 150^3}{6\sin(0.577)} = 34{,}072{,}593\ .22\ \text{mm}^4$$

$$D_y = \frac{EI_y}{q} = \frac{210000 \times 34072593}{1050} = 6{,}814{,}518{,}643.92\ \text{N mm}$$

$$\tau_{cr,G} = k_G \frac{D_x^{0.25} D_y^{0.75}}{t_w h_w^2} = 36 \times \frac{8281690 \times 6814518643}{8 \times 2500^2} = 916 MPa$$

$$\tau_{cr,I} = \frac{\tau_{cr,L}\cdot\tau_{cr,G}}{\left(\left(\tau_{cr,L}\right)^n + \left(\tau_{cr,G}\right)^n\right)^{\frac{1}{n}}} = \frac{805 \times 916}{805 + 816} = 455 MPa$$

The proposed buckling stress of the tapered corrugated web ($\tau_{cr,Prop}$) is given as:

$$\tau_{cr,Prop} = \frac{1.04\tau_{cr,FE,P}}{(1+\tan\gamma)} = 1.04 \times \frac{455}{1+\tan\left(15° \times \frac{\pi}{180}\right)} = 351 MPa$$

$$\lambda_s = \sqrt{\frac{\tau_y}{\tau_{cr,Prop}}} = 0.764$$

The shear strength value ($\tau_{ul,upc}$) of the requested tapered BGCW, finally, is:

$$\frac{\tau_{ul,upc}}{\tau_Y} = 1 - 0.407(\lambda_s - 0.8) = 0.98$$

$$\frac{\tau_{ul,upc}}{\tau_{ul,FE}} = 0.92 \text{ ok.}$$

Chapter 6. Conclusion

In order to apply steel girders with corrugated web plates in practice, their behaviour under shear load needs to be investigated. These girders are used in bridges and large span structures. In order to achieve economical design, the thickness of the web should be as small as possible. However for very thin webs, shear buckling is very likely to happen.

In this thesis, the shear capacity of tapered girders with trapezoidally corrugated webs has been studied, by non-linear FEA. In the FEA, large deflections and material nonlinearity have been taken into account. Also, based on the test results and the FEA, it can be found that the flange does not seem to have much effect on the ultimate shear capacity.

It is generally considered that the contribution of the web to the ultimate moment capacity of a beam with corrugated web is negligible, and the ultimate moment capacity will be based on the flange yield stress. The shear stress along the side of the flange is nearly zero; it is clearly that almost all the shear force is taken by the web.

Like girders with flat webs, web thickness has a significant effect on the shear capacity of the specimen. Girders with thicker webs has higher buckling load. The shear failure is essentially sudden, the local deformation, caused by initial imperfection $h_{w1}/200$. Nevertheless, its accuracy increases for initial imperfections similar to the web thickness (t_w) for cases of $t_w \geq h_{w1}/200$. Those loose the effects of the geometric and material nonlinearity. Also, local imperfection of the web plate caused premature shear buckling instead of yielding of the compression flange.

The out-of-plane deformation of the corrugated webs is relatively limited as a result of their significant out-of-plane stiffness, so the failure mode of the BGCWs does not show the propagation of shear plastic hinges (SPHs) at their top flange similar to those appear in plate girders with flat web plates.

It found that the ultimate shear capacity increases proportionally with the girder depth. So, It can be seen that increasing the inclined flange angle (γ) significantly reduces the ultimate shear strength of the tapered BGCWs, while the initial stiffness remains more or less the same. Additionally, it can be seen that all tapered BGCWs behave in a brittle manner irrespective of the value of γ with a considerable residual strength remaining after failure.

An increase in the $\tau_{ul,FE}/\tau_y$ ratio for tapered BGCWs with the increase of γ. However, the rate of increase becomes higher for girders with increased aspect ratio (a/h_w). This increase results from the reduction in the critical web depth (h_{wo}) which becomes more pronounced in girders with larger a/h_w ratio.

The post-buckling shear capacity not only increases with the girder depth, but also dependent on the ratio of girder length over girder depth. Girders with increased a/h_{w1} ratios are more inclined to shear deformations and, therefore, can relatively reach higher stresses relative to

their plastic shear resistances ($\tau_{ul,FE}/\tau_y$) compared to girders with less a/h_{w1} ratio specially for girders with large angle of inclination.

However, as can be noticed, the $\tau_{ul,FE}/\tau_y$ ratios of the girders with the least inclination angle (i.e. $\gamma = 10°$) seem not to be affected by the change in the a/h_{w1} ratio similar to the case of prismatic girders.
Also, from the load-displacement curves of the models, it can be noticed that the ultimate shear buckling capacity increases with the increase of the web depth. And the stiffness of the beam also increases with the increase of the web depth,

The failure mode of the BGCWs does not show the propagation of shear plastic hinges (SPHs) at their top flange similar to those appear in plate girders with flat web plates. This is because the out-of-plane deformation of the corrugated webs is relatively limited as a result of their significant out-of-plane stiffness. So, no relative shear deformation exits between both flanges to form the SPHs.

It is possible to notice that as the angle between panels decrease, the ultimate shear decreases due to the fact that the web has much more rigidity. It is worth pointing that the web with lower angle among panels has the behaviour as flat panel, as can be seen in figure 26 and 27. Global shear buckling modes have been observed, depending on the web geometry. They also found that the corrugation depth did not seem to have much effect on the ultimate shear capacity but affected the degree of the localization of the buckling mode. It was found that the vertically corrugated web provides a stronger support against the flange buckling than those with horizontally corrugated and plan webs.

Shear capacity equations have been proposed based on classical elastic shear buckling theory and shear yielding, with inelastic transition regions. But the available data are most often based on tests of small beams with flat flange and the material thickness is generally well below what would be expected in practice.

The first region, $\lambda_s \leq 0.6$, is accurately presented, the second, $0.6 < \lambda_s \leq \sqrt{2}$, inelastic region has big variations ranging from conservative to non-conservative results. In the third one $\sqrt{2} < \lambda_s$, in the equation proposed previously by other authors, the proposed equation model provides a lower bound for the shear strength of tapered BGCWs and, generally, it shows suitable predictions in almost practical in first and cases first and third region. According, it will need to modify the equation by raising the curve upwards, regarding equation 28.

References

[1] Ikeda, S., Sakurada, M. "Development of Hybrid Prestressed Concrete Bridges with Corrugated Steel Web Plates", 30th Conference on Our World in Concrete & Structures, Singapore, 23 - 24 August, 2005, Online version: http://cipremier.com/100030003. http://www.hera.org.nz/Story?Action=View&Story_id=1295, 2013.

[2] Yi, J., Gil, H., Youm, K. and Lee, H., "Interactive Shear buckling Behavior of Trapezoidally Corrugated steel webs", Engineering structures, Vol. 30, pp. 1659-1666, 2008.

[3] Moon, J., Yi, J.., Choi, B.H. and Lee, H., "Shear strength and design of trapezoidally corrugated steel webs", Journal of Constructional Steel Research, Vol. 65, pp. 1198-1205, 2009.

[4] Eldib, M.E.A., "Shear buckling strength and design of curved corrugated steel webs for bridges", Journal of Constructional Steel Research, Vol. 65, pp. 2129-2139, 2009.

[5] Hassanein, M.F. and Kharoob O.F., "Behavior of Bridge Girders with Corrugated Webs: (I) Real Boundary Conditions at the Juncture of the Web and Flanges", Engineering Structures, Vol. 57, pp. 554-564, 2013.

[6] Hassanein, M.F. and Kharoob O.F., "Behavior of Bridge Girders with Corrugated Webs: (II) Shear Strength and Design", Engineering Structures, Vol. 57, pp. 544-553, 2013.

[7] Hamilton, RW., "Behavior of Welded Girder with Corrugated Webs", Ph.D. thesis, University of Maine, 1993.

[8] Driver, RG., Abbas HH., Sause R., "Shear Behavior of Corrugated Web Bridge Girders", Journal of Structural Engineering, ASCE, Vol. 132(2), pp. 195-203, 2006.

[9] Bedynek, A., Real, E., Mirambell, E., "Tapered plate girders under shear: Tests and numerical research", Engineering Structures, Vol. 46, pp. 350-358, 2013.

[10] Hassanein, M.F. and Kharoob O.F., "Shear Buckling Behavior of Tapered Bridge Girders with Steel Corrugated Webs", Engineering Structures, DOI: 10.1016/j.engstruct.2014.05.021.

[11] ABAQUS Standard User's Manual The Abaqus Software is a product of Dassault Systèmes Simulia Corp., Providence, RI, USA Dassault Systèmes, Version 6.8, USA,2008.

[12] EN 1993-1-4. Eurocode 3: Design of steel structures – Part 1–4: Plated structural elements - Annex D [informative] – Plate girders with corrugated webs; 2006

[13] Johansson, B., & Maquoi, R. (2007). Commentary and worked examples to EN 1993-1-5" Plated structural elements. Joint Report JRC-, 3(October). Retrieved from http://e-konstrukcije.si/user_files/vsebina/Informacije/Commentary and worked examples to EN 1993-1-5 Plated structural elements.pdf

[14] EN 1993-1-1. Eurocode 3: Design of steel structures – Part 1-1: General rules and rules for buildings. CEN; 2004.

[15] Zárate AV. 2002. PhD Thesis "Un modelo para dimensionamiento de vigas armadas de inercia variable de alma esbelta ", Universitat Politècnica de Catalunya, Barcelona, Spain.

[16] Galambos TV, editor. Guide to stability design criteria for metal structures. New York, NY: John Wiley & Sons, Inc.; 1988.

[17] Easley JT. Buckling formulas for corrugated metal shear diaphragms. J Struct Div, SECF, 1975;ST7:1403–17.

[18] Lindner J, Aschinger R. Grenzschubtragfähigkeit von I-trägern mit trapezförmig profilierten Stegen. Stahlbau 1988;57(12):377–80.

[19] Elgaaly M, Hamilton RW, Seshadri A. Shear strength of beams with corrugated webs. J Struct Eng 1996;122(4):390–8.

[20] Abbas HH. Analysis and design of corrugated web I-girders for bridges using high performance steel. Ph.D. dissertation. Bethlehem (PA): Department of Civil and Environmental Engineering, Lehigh University; 2003.

[21] Sause R, Braxtan TN. Shear strength of trapezoidal corrugated steel webs. J Constr Steel Res 2011;67:223–36.

[22] Gil H, Lee S, Lee J, Lee H. Shear buckling strength of trapezoidally corrugated steel webs for bridges. Transport Res Rec: J Transport Res Board 2005:473–80 [CD 11- S, Transportation Research Board of the National Academies, Washington, DC].

[23] Hassanein MF, Kharoob OF. Shear strength and behavior of transversely stiffened tubular flange plate girders. Eng Struct 2010;32:2617–30.

[24] Research committee for hybrid structures with corrugated steel web. Design manual for PC bridges with corrugated steel web; 1998.

[25] Hassanein, M.F., "Imperfection Analysis of Austenitic Stainless Steel Plate Girders Failing by Shear", Engineering Structures, Vol. 32(3), pp. 704-713, 2010.

ANNEX A: ASPECT RATIO RESULTS OF CASE I AND CASE II FROM MAUPRE BRIDGE.

t_w = 4 mm

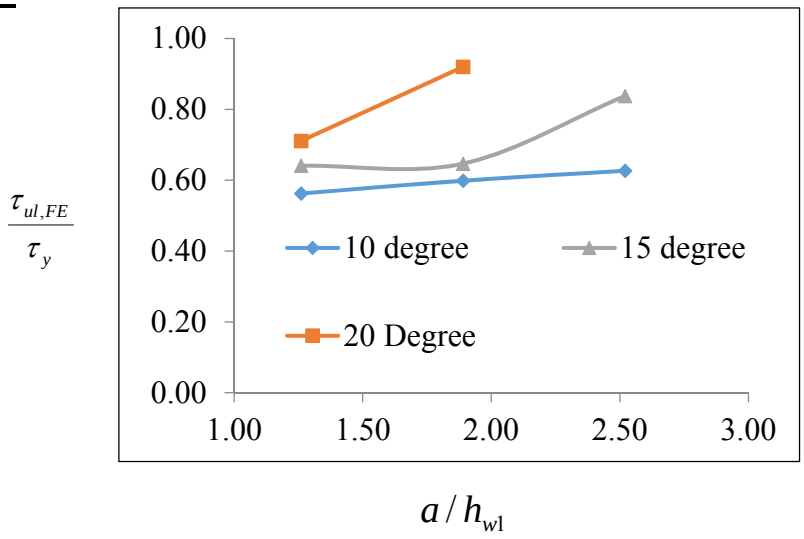

t_w = 6 mm

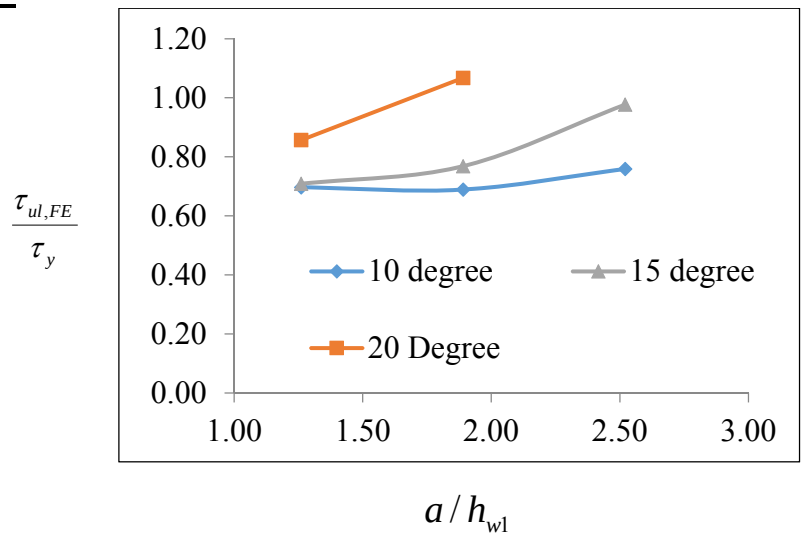

t_w = 8 mm

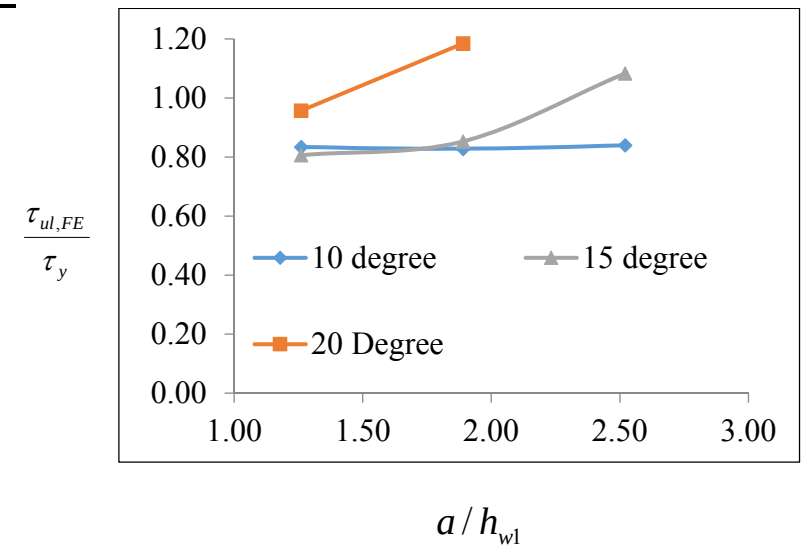

t_w = 10 mm

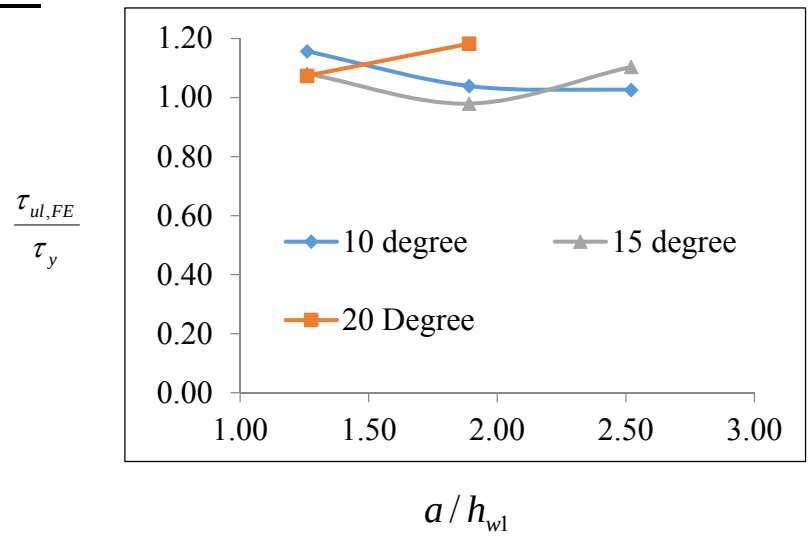

t_w = 12 mm

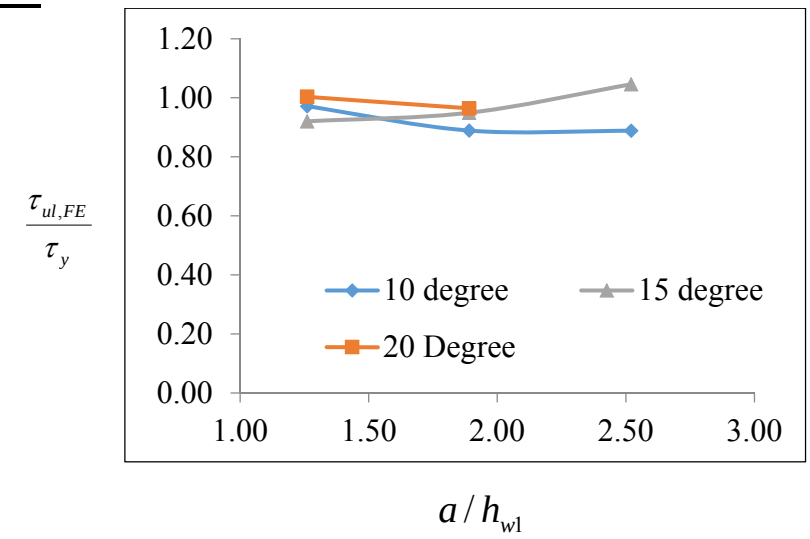

t_w = 14 mm

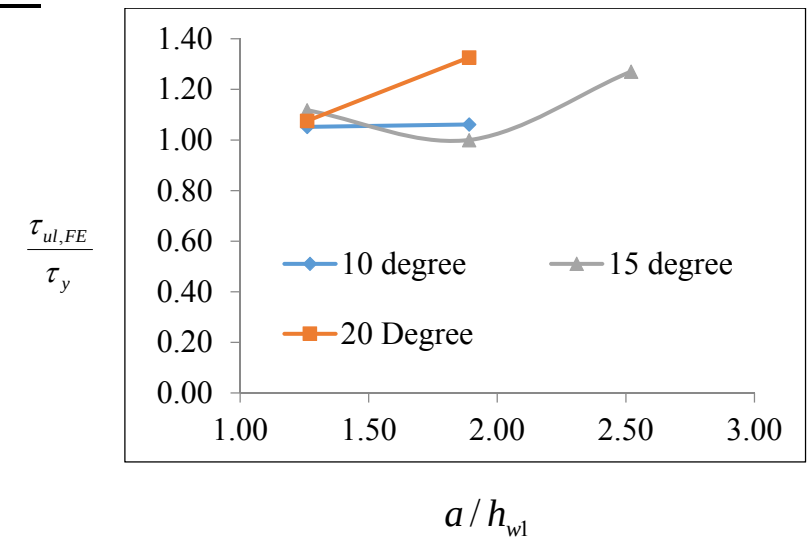

CASE II – MAUPRE BRIDGE

t_w = 4 mm

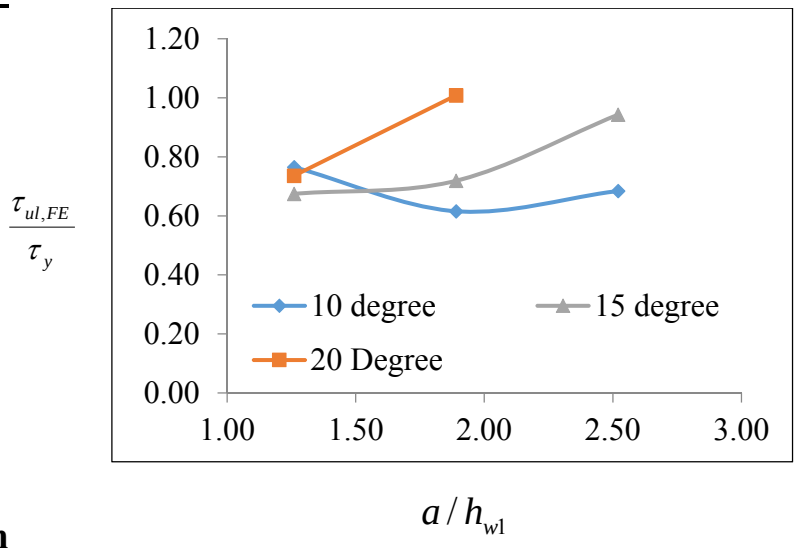

t_w = 6 mm

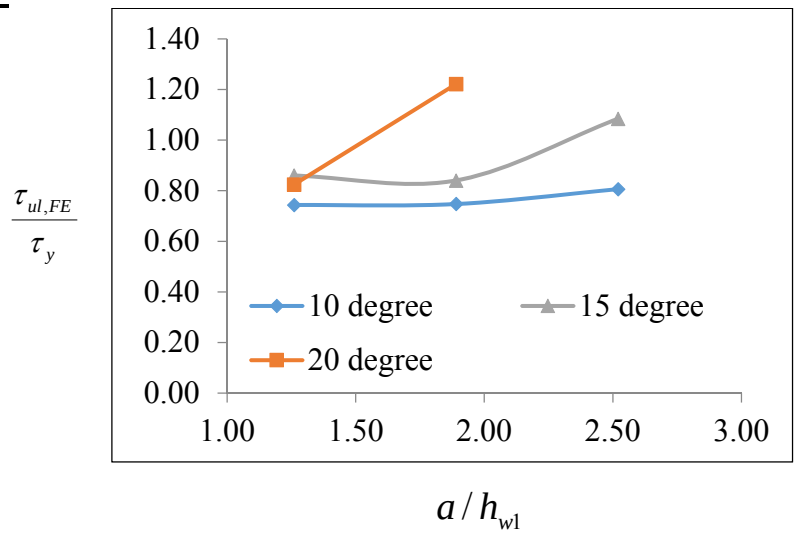

t_w = 8 mm

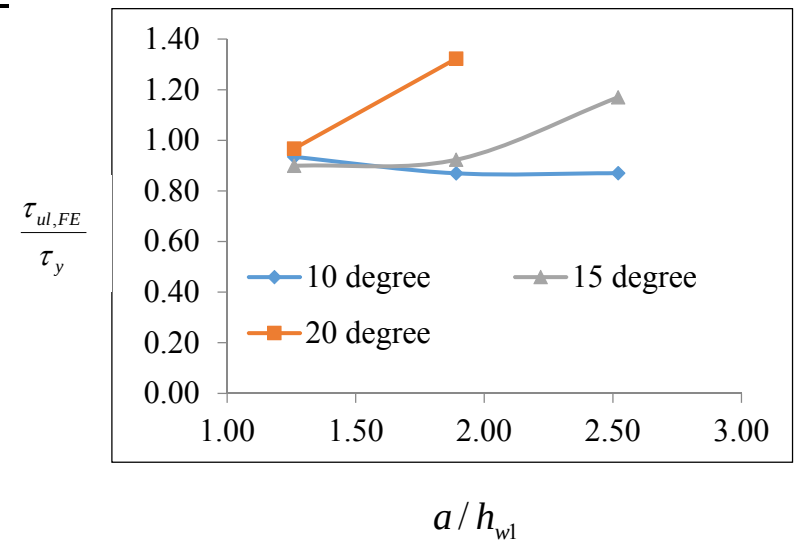

t_w = 10 mm

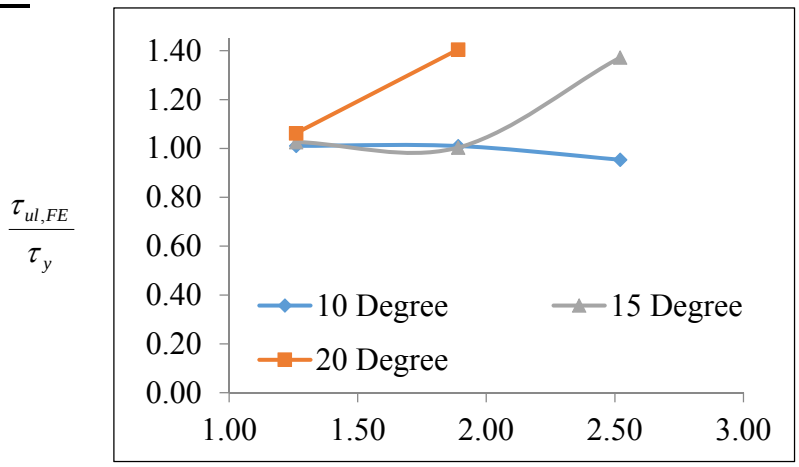

t_w = 12 mm

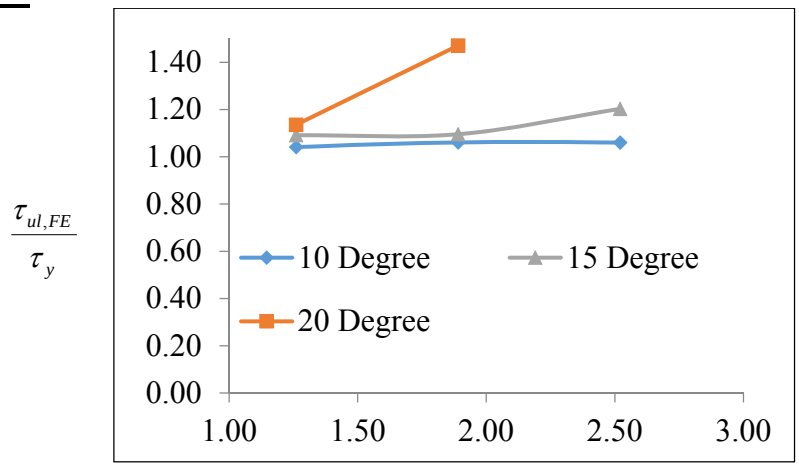

t_w = 14 mm

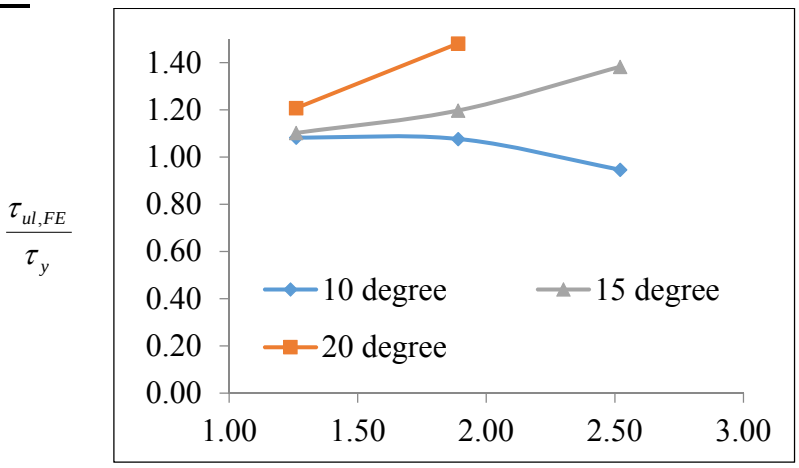

ANNEX B: FLANGE INCLINATION ANGLE RESULTS OF CASE I AND CASE II FROM MAUPRE BRIDGE.

CASE I – MAUPRE BRIDGE

t_w = 4 mm

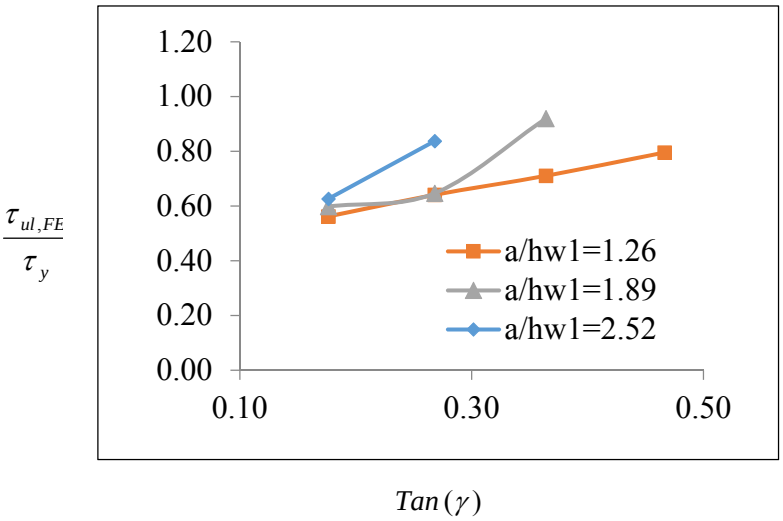

t_w = 6 mm

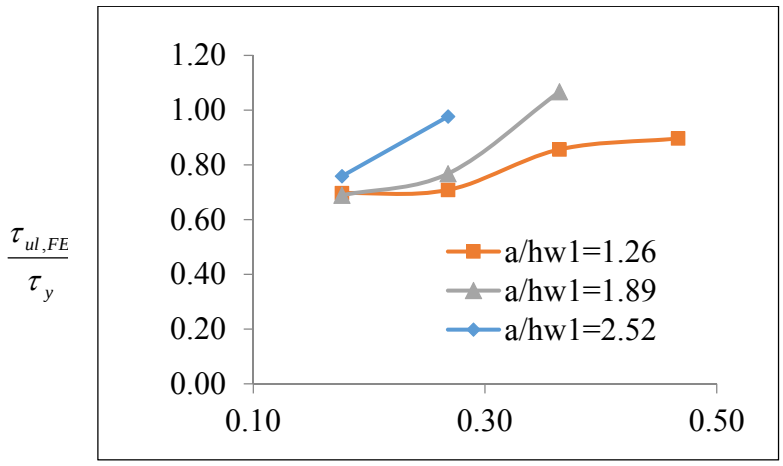

t_w = 8 mm

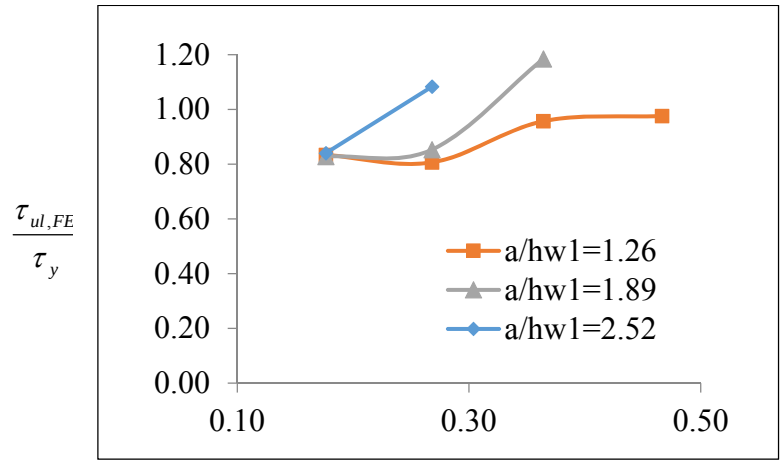

t_w = 10 mm

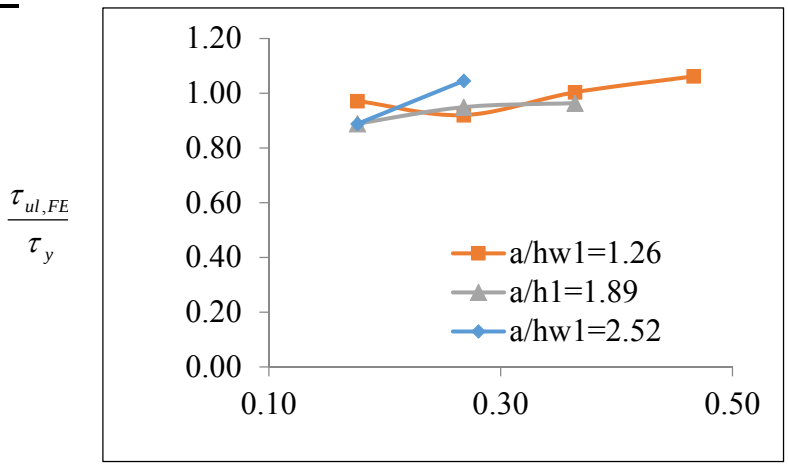

$\frac{\tau_{ul,FE}}{\tau_y}$

$Tan(\gamma)$

t_w = 12 mm

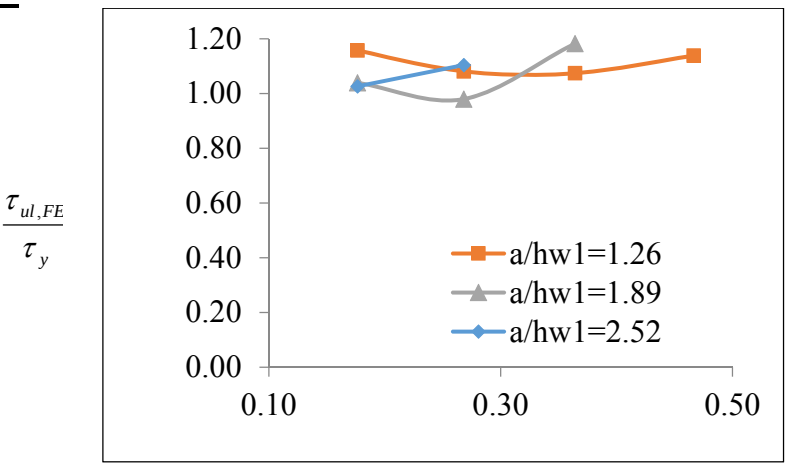

$\frac{\tau_{ul,FE}}{\tau_y}$

$Tan(\gamma)$

t_w = 14 mm

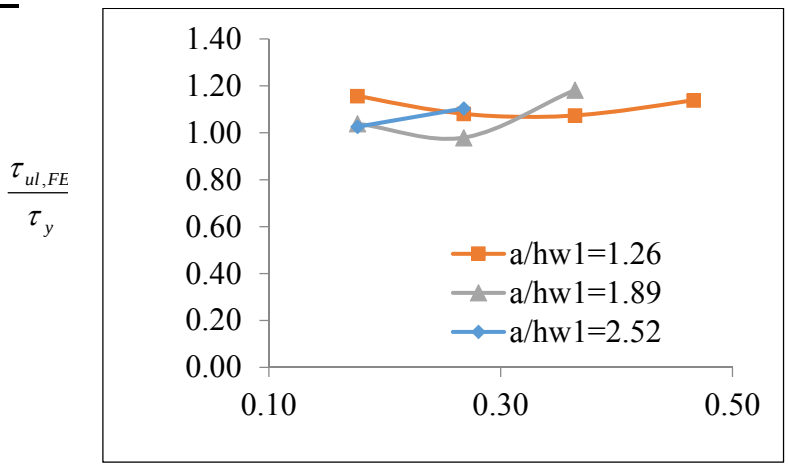

$\frac{\tau_{ul,FE}}{\tau_y}$

$Tan(\gamma)$

CASE II – MAUPRE BRIDGE

t_w = 4 mm

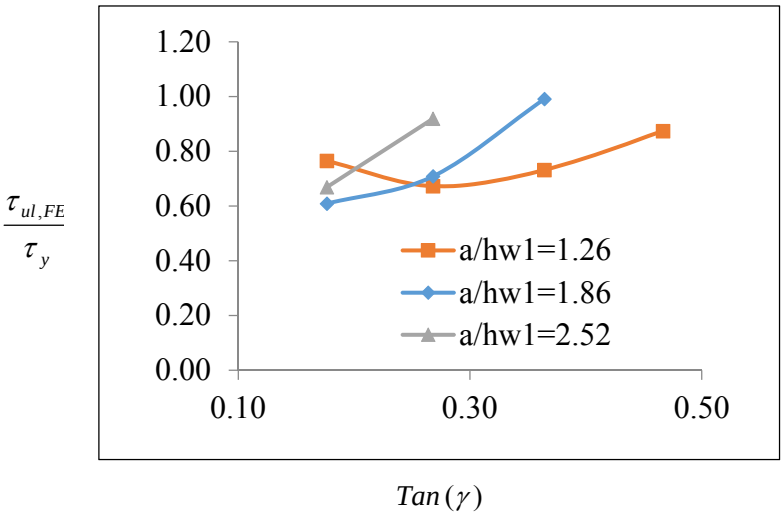

t_w = 6 mm

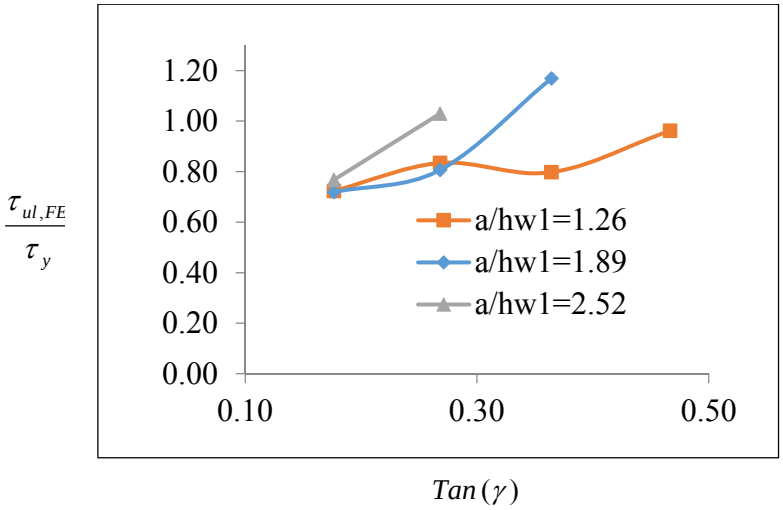

t_w = 8 mm

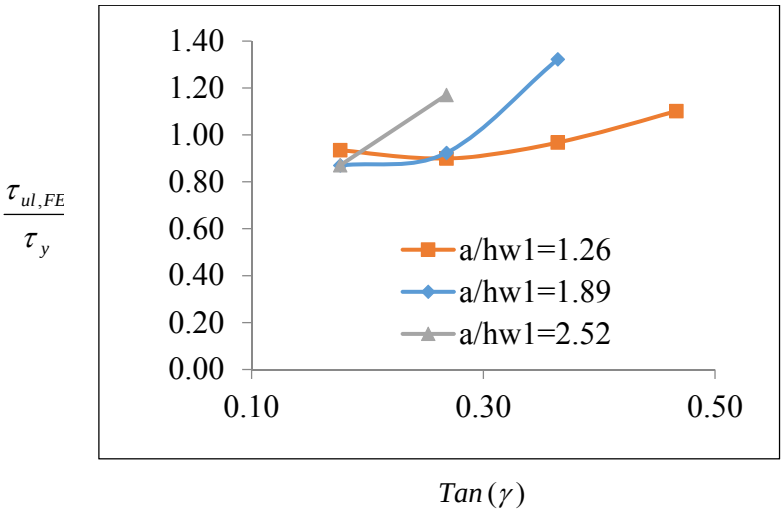

t_w = 10 mm

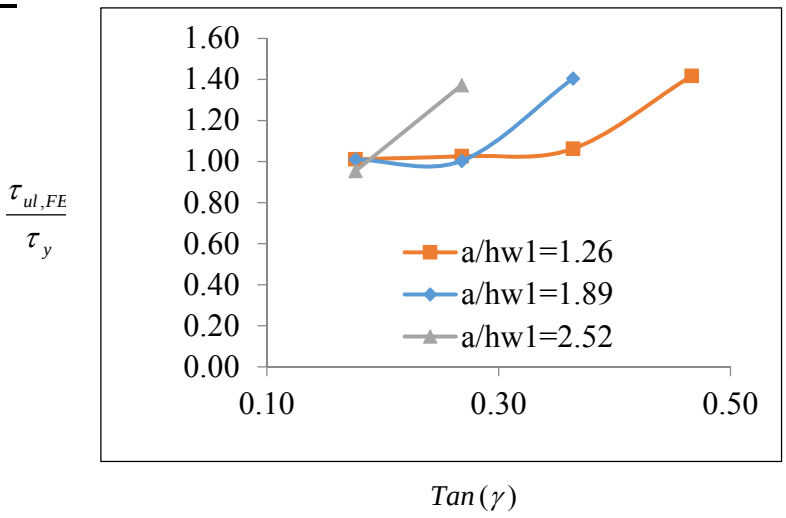

t_w = 12 mm

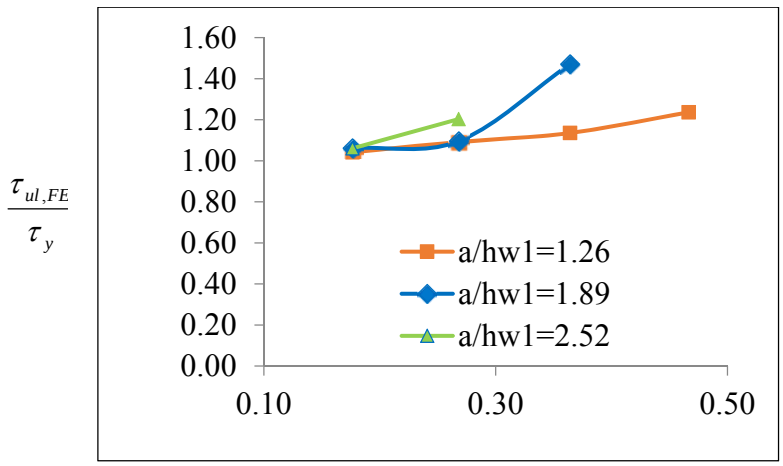

t_w = 14 mm